

Anonymous Referee #1

*Below are the comments from the referee in **black** and replies from the authors in **blue***

General Comments

This manuscript presents the data and analyses of balloon-borne measurements from Northern India and on the southern slope of the Tibetan plateau during two Asian summer monsoon (ASM) seasons. The high vertical resolution profiles of temperature, water vapor, ozone, as well as the cirrus clouds and aerosol information are analyzed together to characterize the region's UTLS thermal and dynamical structure, transport characteristics, in particular the transport of water vapor into the stratosphere and the presence of the Asian tropopause aerosol layer (ATAL). This work is part of a larger project involving the airborne campaign StratoClim. The data and the analyses are well documented in the manuscript. The result contributes important new information to the larger picture of ASM UTLS transport. The work is high quality and fits the scope of ACP well. I have a number of suggestions for improving the manuscript, mostly related to presentations and discussions of the results.

We are grateful to Anonymous Referee #1 for the careful reading and for providing many valuable suggestions, which contribute to improving the manuscript significantly.

We recognize that the points raised by the reviewer about the 3D structure of ASMA are valid, and particularly relevant for assessing the moistening mechanisms of the CLS. This issue is now addressed in the conclusions, with considerations about adiabatic transport from the Tibetan plateau to the southern slopes of the Himalayas and CPT variability based on existing literature. We also recognize that the assessment of the ASM role in moistening the stratosphere is only partly supported by the analysis in this paper, which does not take into account horizontal motion of the air, and consequently this statement was revised in the conclusions.

The abstract was revised in order to better highlight the objectives of this paper, namely to provide an overview of all the balloon measurements performed during our campaigns and to address the broad relevance of this dataset. More targeted studies addressing the question of stratospheric moistening are still ongoing, and the results will be discussed in future publications.

As suggested by the reviewer, the meteorological overview was improved, in particular the seasonal variability section and Figure 2, now showing time-averaged cross sections (including the easterly jet position) and geopotential height fields along with the trajectories. We made the formulation of the proposed UTLS structure more handy by rearranging Sections 4.3-5.2 and introducing the schematics (now Figure 6) earlier in the paper. This includes reducing the use of not well established acronyms (now also summarized in Table 1) and avoiding redundancy in figures (comparison with ECMWF figure removed). The revised manuscript is more concise than the previous version, which was achieved by avoiding repetitions (e.g. campaign specifics) and making the overall discussion more targeted to the objectives of this paper.

In the following, we reply point-by-point to the reviewer's comments, and highlight the corresponding changes made to the manuscript. Note that page and line numbers given in the replies refer to the revised version of the manuscript without tracked-changes.

Major comments and suggestions:

1) Balloon-borne measurements have their strengths and weaknesses. When making interpretation, it is important to recognize the main weakness that the data is approximately one dimensional while the atmosphere in general is described in 3 (spatial) + 1 (time) dimensions. In this specific study, the location of measurements is uniquely situated in the region of steep elevation change.

Associated with the terrain variation, the upper level anticyclone also creates a significant tropopause height variation. How the measurement location is relative to the horizontal structure of the tropopause height, especially the region of the highest tropopause, is very important for the conclusions. This consideration is largely missing in the discussion.

Suggestion: Discuss your results in contrast to the results from previously published work using data from balloon-borne measurements with similar payloads but launched from the Tibetan plateau (Bian et al., 2012). Identify the key differences and their implications to your conclusions in relation to the UTLS structure.

We agree with the reviewer that considering the 3D structure of ASMA, and particularly the “bulging” CPT above the Tibetan plateau, is important for assessing the mechanisms moistening of the CLS. The fact that isentropic transport from Tibetan plateau / below CPT to southern slopes of Himalayas / above CPT might be responsible for (part of) the enhanced H₂O observed in the CLS is an important feature that was missing in our previous discussion. This issue is now discussed in the conclusions section, based on comparison of the average CPT isentropic levels from our datasets with Tibetan plateau soundings from Bian et al. (2012) as well as with considerations about CPT variability based on previous literature (page 14, lines 3-9).

Comparison of our southern-slopes measurements with the simultaneous Lhasa 2016 and Kunming 2017 campaigns of SWOP in the Tibetan plateau region are ongoing (see page 15 lines 1-2) and the results, which will address explicitly the issue of adiabatic transport vs slow ascent and overshooting convection (i.e. “chimney vs blower”), will be discussed in a future publication.

2) When concluding the role of ASM in moistening the stratosphere, it is important to recognize that the time scale changes at the level around the CPT. While the vertical transport up to the CPT is in general within the season, it becomes much slower above. The significant difference between the “confined layer” and the “background stratosphere (FLS)”, defined to be above the level ~ 65 hPa, is part of the “tape recorder” structure, i.e. the summer and winter difference. How does the ASM enhance this difference is the relevant question.

Suggestions: For the structure of the water vapor tape recorder, a good recent figure could be the Fig.2 of Glanville and Birner (2017). To estimate how much ASM is more effective in moistening the stratosphere compared to the tropical equatorial entry point in summer, you could possibly use the published result in Bian et al., 2012 (Fig 5) where soundings from Costa Rica (TC4) are used as a contrast to the ASM.

We agree with the reviewer that, for assessing the role of ASMA in moistening the stratosphere, comparing different stacks of altitudes is of limited use due to the tape recorder structure, and that the fate of the enhanced H₂O observed in the CLS needs to be addressed by explicitly taking into account the horizontal motion of the air.

Consequently, the comparison of water vapor PDFs in the CLS and free stratosphere region was removed from the manuscript, and replaced with a discussion based on results from recent literature (namely, Pan et al., 2016) (page 14 lines 10-17). In this paragraph, the statement of ASMA moistening the stratosphere is flagged as “potential” (page 14 line 10).

As mentioned in the manuscript (page 2 lines 5-6 and page 14 lines 32-33), further investigations aimed to assess the relevance of our measurements in the context of stratospheric moistening and related processes are currently ongoing. However, we refrain from performing additional analyses here, as we intend to discuss this issue in a future dedicated publication.

Additional comments:

3) This manuscript is desired to be more concise. For example, it is not clear how section 3 is contributing to the goal of the paper, since the discussion there are not related to particular scientific questions. The points made in that section may be better received when addressing particular questions in the later sections. Also suggest that you work to reduce the repetition of figures.

Suggestions: Be clear on the key objectives of the paper and focus on what serves these objectives. For example, is the comparison of the mean profiles with ECMWF necessary for the objective? Also note that some campaign specifics appeared three times (abstract, intro and campaign description).

Several minor and major changes were made in order to make the manuscript more concise and more targeted to its objectives, and to avoid redundancy in figures. In particular:

- Abstract simplified (use of acronyms reduced)
- Figure 4 (comparison with ECMWF) removed
- Figure 6 reduced (panel a eliminated, panel b given as Figure S4 in supplementary material)
- Use of acronyms reduced (FLS eliminated, use of UT and LS as individual acronyms avoided)
- Main acronyms summarized in Table 1
- Sections 4.3-5.2 rearranged and schematics figure introduced earlier in the paper (Figure 6)
- Campaign specifics removed from abstract and introduction

As a consequence, the revised manuscript is shorter than the previous version (despite several other additions requested by the reviewers were made), and we believe the presentation of the UTLS structure that we define is more fluent and reader-friendly.

4) When describing the dynamical settings and seasonal changes, it is important to connect to the seasonal change of the ITCZ. See schematic in Lawrence and Lelieveld (2010) and Pan et al 2016 for related discussions. This will put the change from August to November into the right context. It is also more desirable to show the cold point tropopause in ECMWF in addition to PV, since CPT is what you use with the observation.

According to this comment, the discussion of dynamical settings and seasonal variability was improved with references to Lawrence and Lelieveld (2010) and Munchak and Pan (2014), relating the observed features to the seasonal variations of the ITCZ and the jet streams (page 5 lines 22-23, page 5 lines 30-32 and page 7 lines 14-16). In addition, a sketch of the ITCZ is now shown in schematics of the UTLS structure (Figure 6). Figure 2 was also improved to facilitate the discussion of the seasonal variability (see details in specific comment below).

Specific comments and suggestions:

- References:

P2L13: consider replacing Park 2007 by Hoskins and Rodwell 1995.

Done (page 2 line 10).

P2I23: add Ungermann et al., 2013 before Fadnavis

Done (however, note that it is Ungerman et al., 2016, added after Fadnavis et al., 2013 to maintain chronological order) (page 2 line 19).

- Wordings:

P1L22: "It is known to be enriched" -> "It is observed from satellite to contain enhanced"

Done ("be enriched" -> "contain enhanced") (page 1 line 22).

P1L24: remove "very"

Done (page 1 line 25).

P2L4: reconsider "depletion" – the low ozone is not due to depletion but lofted low ozone air.

The whole sentence was removed in new abstract.

P3L11: rephrase "notoriously hardly accessible"

Done (page 3 line 9).

P5L2: rephrase "too high" F. P. temperature and "too high" w.v. mixing ratio. Perhaps "w.v. mr derived by the f. p. t. are too high to be physical"?

Done (page 4 lines 32-33).

P14L26-28: A more accurate statement here should be "it is interesting to contrast the result from Pan et al. 2014, where a smaller variability of water vapor is found above the CPT ..." Comparing the water vapor range of variability in Pan et al. 2014 (figs. 6&7, _ 3-5 ppmv) with results from this work (DK17 is _ 3.5-6.5 ppm, and NT16 is similar to the Kunming), the variabilities are qualitatively the same. Not sure where you found the "no variability above CPT" as a common concept.

The whole sentence was removed in new conclusions section.

- Figures:

Fig.2: (a) Consider adding easterly jet, which will show where the sounding location was in relation to the anticyclone. (b) Also consider adding simple dynamical field, GPH or tropopause 100 hPa contour to the maps on the right to indicate the anticyclone and possibly the region of highest tropopause. (c) it may be more insightful to color the trajectories by potential temperature.

Figure 2 was subject to a number of improvements accordingly:

- Wind contours at 20 m/s and 30 m/s added, showing the easterly jet position (panels a-c-e)

- X-axis range enlarged to show latitudes 10-50°N (panels a-c-e)

- Individual days replaced with time-average of the respective campaign periods (panels a-c-e)

- Geopotential height at 100 hPa (time average of each measurement period) added to the trajectory panels, showing the region of highest tropopause (panels b-d-f)

As a consequence, Figure 2 now provides a significantly higher amount of information than the previous version, and the discussion of seasonal variability was improved accordingly (page 6 line 26 to page 7 line 6).

Figs. 6-7: there is a strong discontinuity between the two figures when you changed from pressure to altitude. Suggest you consider using pressure altitude when you can label the profiles using both pressure and altitude. This can be consistently done throughout the paper.

Unfortunately we do not understand this comment properly, and in particular it is not clear to us what the reviewer means by “discontinuity”. Figure 7 shows altitude relative to CPT as y-axis (not just altitude), therefore adding an altitude scale to all plots would not make the profiles look more similar. In addition, all figures in the paper show more than one dataset at the same time, hence adding an altitude axis along with the pressure profiles is strictly speaking not possible. Therefore, we refrain from applying any changes.

Fig. 8. There is an error in the caption: FLS should not be CPT to CPT+5 km. By definition, FLS is above the TOC. I hope this is only an error in description, not in the actual calculation.

The reviewer is right and the description was corrected accordingly (the actual calculation was correct). Note that the definitions of the free stratosphere and troposphere regions for the PDFs calculation are now given in Section 5.3 (page 10 lines 2-4) instead of in the caption of Figure 8.

Anonymous Referee #2

*Below are the comments from the referee in **black** and replies from the authors in **blue***

General comments

Brunamonti et al. present results from the StratoClim balloon campaigns. They measured vertical distributions of temperature, ozone, water vapour and aerosol in the south Asian UTLS during one post-monsoon and two monsoon campaigns. They identify three significant thermodynamic levels and layers, which provide a framework to understand the UTLS structure within the Asian summer monsoon anticyclone. The paper is sound and clearly within the scope of ACP(D). It is based on a new and important data set that needs to be published.

Some arguments regarding the confinement effect of the ASMA are not yet clear to me, or at least do not sufficiently consider alternative explanations: Convective height might primarily control H₂O, O₃, and confinement. The effect of confinement on H₂O and O₃ needs to be clarified. Details are given in the specific comments.

It's hard to tell whether addressing those requires minor or major revisions. Alternatively, the paper would be worth publishing even without discussing the relative importance of confinement and other processes in the ASMA. The outlook at the end of the paper shows its importance for ongoing other studies.

We are grateful to Anonymous Referee #2 for the careful reading and for providing many valuable suggestions, which contribute to improving the manuscript significantly.

We recognize that the points raised by the reviewer concerning the relative importance of confinement and convective altitude are valid, as well as the considerations made in specific comments regarding age of air and convection. We improved the discussion of the H₂O, O₃ and aerosol vertical distributions by taking into account the suggested alternative explanations (mainly Sections 5.3 and 6.2), and our conclusions were revised accordingly.

As suggested by the reviewer, the use of acronyms was reduced for easier reading (including the abstract, which was substantially simplified) and redundancy in figures was avoided. A new table was introduced to summarize the main not well established acronyms (Table 1). The formulation of the UTLS structure that we propose was made more fluent by rearranging Sections 4.3-5.2 and by introducing the schematics figure (now Figure 6) earlier in the paper.

The meteorological overview section was also improved, and particularly Figure 2, now displaying time-averaged cross sections and geopotential height fields along with the trajectories.

Despite several additions (requested by the reviewers) were made, the revised manuscript is more concise than the previous version. This was achieved by avoiding repetitions (e.g. the campaign details) and making the overall discussion more targeted to the objectives of this paper.

In the following, we reply point-by-point to the reviewer's comments, and highlight the corresponding changes made to the manuscript. Note that page and line numbers given in the replies refer to the revised version of the manuscript without tracked-changes.

Presentation

(1) Too many acronyms make the paper hard to read. I suggest to count the number of occurrences of each (not well established) acronym, then write out those 50 % that occur least.

The use of acronyms was reduced in the manuscript accordingly, namely by eliminating FLS (free lower stratosphere) and avoiding the use of UT and LS as individual acronyms (e.g. CLS is now used consistently throughout the whole paper, avoiding the use of "Confined LS"). In addition, a new table was introduced to summarize the main not-well established acronyms used in the paper

(Table 1), and the schematics in former Figure 13 was introduced earlier in the paper (now Figure 6) to help the reader familiarize with the acronyms.

In order to make the manuscript more reader-friendly and the formulation of the UTLS structure that we propose more fluent, we have also moved former section 4.3 (“Horizontal confinement in ASMA”) to section 5.3 (“Confined lower stratosphere”), where the acronyms TOC and CLS are defined and the schematics in Figure 6 is discussed.

Finally, the abstract was also simplified by strongly reducing the use of acronyms in it.

(2) Consider to reduce redundancy in the figures (e.g. T vs p for DK17 and NT16AUG is shown in Figs. 1, 4, 6a, 13).

Redundancy in figures was reduced accordingly:

- Figure 4 (comparison with ECMWF) was removed, as it was not directly necessary to the objectives of the paper

- Figure 6 reduced: panel a (T vs p) was removed due to redundancy, and panel b (θ vs p) moved to supplementary material (Figure S4).

(3) Consider to annotate curves etc. in the figures only, rather than the captions. For instance in Fig.13, the campaigns and the meaning of the colours impede reading of the caption, but are already obvious from the panels.

In Figure 13 the curves are identified by the color of their axis label, and since the figure is already quite “full”, we believe there is no need to add an extra legend to it (we tried different options but figure becomes too hard to read). In the revised version, Figure 13 was improved with respect to the previous version (θ dashed lines changed from green to grey, labels rearranged).

Specific comments

Line numbers in the following are approximate, sometimes referring to the arguments of an entire paragraph.

P3L7: What about aircraft measurements? CARIBIC provides a lot of species in high resolution. Dedicated campaigns (ESMVal/HALO, OMO/HALO, StratoClim/Geophysica) sampled higher altitudes and also did some profiles. There are a few aircraft in-situ monsoon papers, at least from CARIBIC and ESMVal.

Reference to aircraft measurements in ASMA, namely from ESMVal (Gottschald et al., 2018) and CARIBIC (Raute-Schöch et al., 2016) added to the introduction accordingly (page 3 lines 9-11).

P7L2: Fig. 2 shows snapshots of individual days. Are those days chosen to be representative in some respect? Please consider to provide time averages for the respective measurement periods (or for the sounding days).

Change made accordingly: individual days replaced by time average of each measurement period (Figure 2, panels a, c, e).

P7L9: There are different PV thresholds for the dynamical tropopause. Please provide a reference or justify your choice.

Reference to Kunz et al. (2011) for the choice of the PV threshold for the dynamical tropopause was added, and the discussion was revised accordingly: we now use $PV = 3-4$ PVU which is more appropriate for the considered latitude and season (page 7, lines 5-6).

P7L17: Given the structural differences of the tropopause region between summer and autumn: Why do you choose the same pressure altitude to compare the two seasons? You might consider to show trajectories started over some altitude range, or from a specific distance to the respective tropopause altitudes.

Figure 2 is meant to illustrate the differences between the UTLS structure and dynamical features of the monsoon vs. post-monsoon season in a qualitative manner. The contrast between monsoon and post-monsoon season is already evident by comparing panels b-f vs. panel d (furthermore now that geopotential height fields are also shown in addition to trajectories). Therefore, we believe that there is no need to further refine the trajectory comparison.

P8L23: What is the spacing between trajectory starting points?

Trajectories are initialized at 5 hPa intervals. Manuscript modified to include this information (page 9 line 5).

P8L26: The ASMA box seems to be rather big. Please justify or provide a reference.

Our ASMA box definition (10-50°N, 0-140°E) is based on the average geopotential height fields during our campaign periods, now shown in Figure 2 (page 9 line 11 rephrased accordingly).

Similarly large domains were used to approximate the ASMA area in previous literature, e.g.:

- 15-45°N, 5-105°E (Vernier et al., 2011)
- 10-60°N, 10-160°E (Ploeger et al., 2015)
- 0-60°N, 0-140°E (Pan et al., 2016)

Therefore we believe our boundaries provide a reasonable approximation of the ASMA area.

P9L19: Formulation for O3 is ambiguous. Please revise.

The whole sentence was removed from the revised version (for the sake of brevity).

P10L25: What do you mean by “feature” here: H₂O max, O₃ min, or the combination of both? Anyway, neither the H₂O feature, nor the O₃ feature is necessarily related to differences in the strength of convection alone. The time since the last convective influence on the air mass might also be important. If NT16Aug by chance sampled older air on average, the H₂O feature would have been smoothed out. Also, convection increases the availability of O₃ precursors, leading to enhanced photochemical O₃ production. The absence of an O₃ minimum just above the LRM in NT16Aug might be due to longer confinement or to higher O₃ production. Please discuss.

We agree with the reviewer that considering the age of air (meant as time elapsed since the last convective influence) is important due to enhanced photochemical O₃ production in ASMA, and that the fact of missing O₃ minimum above the LRM in the mean profile of NT16_{AUG} is consistent with older air sampled on average during this campaign vs. fresh convective outflow sampled more frequently during DK17. We also recognize that the same argument applies to the H₂O maximum above the CPT (see comment below).

Assuming the balloon soundings are frequent enough to be statistically representative of the respective measurement periods, we still would argue that this evidence does suggest that more frequent deep convection occurred during DK17 compared to NT16_{AUG}.

The manuscript was revised according to this consideration (page 10 lines 21-26).

P11L5: This is consistent to older samples in NT16Aug.

Same arguments as in the comment above applies to the H₂O maximum above the CPT in DK17: we agree with the reviewer and the manuscript was modified accordingly (page 10 lines 24-25).

P11L8: This argument is not quite clear to me. H₂O in the CLS is compared to H₂O in higher altitudes. The difference is attributed to the horizontal confinement effect of the ASMA. However, first order this might just reflect the decreasing frequency of convective tops with altitude. To quantify horizontal (isentropic) confinement, you might consider comparing back-trajectories according to their respective lengths in the ASMA. Please discuss.

We agree with the reviewer that, to some extent, decreasing “convective signature” with altitude might simply reflect the decreasing frequency of overshooting convective tops with altitude. Indeed, the current status of our analysis does not explicitly disentangles the effects of convective vs. confinement top height in controlling the vertical distributions of H₂O, O₃ and aerosols above the CPT. Furthermore, the anticyclonic confinement is caused by the high pressure built up by the deep convection, hence the two processes are intrinsically connected.

However we also consider that, to our knowledge, convective updrafts overshooting the CPT by 1.5-2 km were never observed (also not by the Geophysics campaign during StratoClim in Nepal), and that the gradients in the vertical distributions of H₂O, O₃ and aerosols are in good agreement with the TOC inferred from backward trajectories.

Therefore, we still would argue that these evidences suggest that the horizontal confinement effect of ASMA plays an important role in shaping the vertical distributions of H₂O and O₃ above the CPT (and in particular the H₂O enhancement in the CLS). Nevertheless, we recognize that further analysis would be required to fully disentangle the relevance of the different transport processes, and we revised the manuscript accordingly (page 10 line 32 to page 11 line 5).

P11L14: Not necessarily, see previous comments on convective strength versus age. Age is related to confinement. Please disentangle.

Same as above: we agree with the reviewer and the manuscript was modified accordingly (page 10 lines 25-26).

P11L16: Confinement tends to increase O₃ via photochemical production. Please discuss horizontal confinement versus the altitude profile of convective influence. The argument regarding the quality of the TOC definition could go the other way round i.e. (simplified): ASMA is driven by convection -> convection reaches to a certain altitude -> no confinement above convective influence.

Same as above: we agree (at least to some extent) with the reviewer, and the manuscript was modified accordingly (page 11 lines 3-5).

P11L20. Ditto.

Same as above: the statement that TOC controls the vertical distributions of H₂O and O₃ was removed and replaced with a more detailed discussion (page 10 line 32 to page 11 line 5).

P11L28: Could different temperatures or different ages (time since last convective influence) be alternative explanations for the difference between DK17 and NT16Aug?

We believe that different temperatures are the main driver of the different ice saturations measured during NT16_{AUG} and DK17, as it is stated already in the manuscript (page 11 line 9). At the current status of our analysis, it is not obvious to infer a correlation between of age of air and ice saturation. The statement that higher ice saturations in DK17 are related to stronger convective activity was removed from the manuscript.

P12L19: Comparing NT16Aug to NT16Nov per se generally reflects seasonal variation. Air mass origins might be totally different in August and November, even if there was no ASMA confinement in August. Please reformulate or elaborate, why NT16Aug without ASMA would be like NT16Nov.

We fully agree with the reviewer that, in addition to confinement (or lack of thereof), air mass origin and potential direct exposure to deep convection is important, as it provides the supply of aerosols and precursor gases to the UTLS. The manuscript was revised accordingly (page 12 lines 1-3).

P12L29: The parameters affecting the threshold depend on region and season. Is the threshold of Vernier et al. applicable to your measurements without adjustments?

The parameters affecting the cloud-filtering thresholds are independent of region and season. These thresholds are just based on optical considerations and the typical size ranges of atmospheric aerosols and ice crystals (see page 12 lines 10-12). Furthermore, it happens that the thresholds by Vernier et al. (2015) have been developed based on measurements from the same region and season as our measurements (Lhasa, China during the ASM season), and comply with CALIPSO depolarization criteria. Therefore, we are confident that these thresholds are applicable to our measurements without adjustments.

P13L21: Could the thermodynamic conditions at the CPT enhance aerosol formation from gaseous precursors? In that case convective outflow or confinement might not be as important.

We agree with the reviewer that thermodynamic conditions (namely colder temperatures) at the CPT can enhance the partitioning of condensable material (e.g. nitrate) to the aerosol phase, and therefore the fact that ATAL shows maximum BSR at the CPT is likely also influenced by temperature, in addition to confinement. The manuscript was revised accordingly (page 13 lines 5-7).

P13L22: "its level": Does this refer to confinement or aerosol enhancement? Please reformulate.

Maximum strength refers to confinement. Sentence rephrased accordingly (page 13 lines 5-7).

P13L25: There is no convective supply of aerosols/precursors in November. Additionally there is no confinement. The ASMA might to some degree enhance ATAL. Consider revising to clarify causes and effects.

Same as discussed above: we agree with the reviewer that supply/lack of aerosols and precursors via deep convection needs to be considered in addition to confinement. Sentence revised accordingly (page 13 line 12).

P14L33: Please also discuss alternatives to confinement.

Alternatives to confinement (supply/lack of aerosols and precursors via deep convection) already discussed in Section 6.2 (see comments above). Conclusions revised accordingly (page 14 lines 18-20).

P15L3: Please discuss convective height versus confinement.

Convective height vs. confinement already discussed in Section 5.3 (see comments above). Conclusions revised accordingly (page 13 line 30 to page 14 line 2).

P15L6: Comparing different altitudes is of limited use for estimating the effects of confinement.

As discussed above, we agree with the reviewer that comparing different altitudes is of limited use for estimating the effects of confinement. This statement was removed from the conclusions.

P15L7: Please also consider convective height and possible vertical variations of aerosol formation.

Same as above: alternatives to confinement (convective height, supply/lack of aerosols and precursors via deep convection) now discussed throughout Sections 5.3 and 6.2. This statement was removed from the conclusions.

P24, Fig. 2: White contours for water vapour are not discernible. Please revise, e.g. consider omitting or doing an extra plot for them. Insets in panels a, c, e are too small. Consider to include those lines in the right column's panels.

White contours for IWC eliminated in the revised version of Figure 2.

P25, caption of Fig. 2: "Note that in panel c (NT16Nov), trajectories started : : :"

- Panel c is not about trajectories.

- stared -> started

- ppm -> ppm

Caption of Figure 2 revised and typos corrected.

P27, Fig. 4: Consider to use ECMWF data only from the times of the respective soundings.

Figure 4 was removed for the sake of reducing redundancy in figures.

P30, caption of Fig. 6: Consider to give a short explanation of "GPS geometric altitude"

Former Figure 6 (now Figure 4) was revised and the caption rephrased to avoid mentioning "GPS" geometric altitude, but just "geometric altitude" as it is done previously in the main text (see page 5 line 12).

Balloon-borne measurements of temperature, water vapor, ozone and aerosol backscatter at the southern slopes of the Himalayas during StratoClim 2016-2017

5 Simone Brunamonti¹, Teresa Jorge¹, Peter Oelsner², Sreeharsha Hanumanthu^{3,4}, Bhupendra B. Singh³, K. Ravi Kumar^{3,10}, Sunil Sonbawne³, Susanne Meier², Deepak Singh⁵, Frank G. Wienhold¹, Bei Ping Luo¹, Maxi Böttcher¹, Yann Poltera¹, Hannu Jauhiainen⁸, Rijan Kayastha⁶, Jagadish Karmacharya⁹, Ruud Dirksen², Manish Naja⁵, Markus Rex⁷, Suvarna Fadnavis³ and Thomas Peter¹

10 ¹Institute for Atmospheric and Climate Science (IAC), Swiss Federal Institute of Technology (ETH), Zürich, Switzerland

²Deutscher Wetterdienst (DWD) / GCOS Reference Upper Air Network (GRUAN) Lead Center, Lindenberg, Germany

³Indian Institute of Tropical Meteorology (IITM), Pune, India

⁴Forschungszentrum Jülich (FZJ), Institute of the Energy and Climate Research – Stratosphere (IEK-7), Jülich, Germany

⁵Aryabhata Research Institute of Observational Sciences (ARIES), Nainital, India

15 ⁶Kathmandu University (KU), Dhulikhel, Nepal

⁷Alfred Wegener Institute (AWI) for Polar and Marine Research, Potsdam, Germany

⁸Vaisala Oyj, Vantaa, Finland

⁹Department of Hydrology and Meteorology (DHM), Kathmandu, Nepal

¹⁰Now at Centre for Atmospheric Sciences, Indian Institute of Technology (IIT), Delhi, India

20 Correspondence to: Simone Brunamonti (simone.brunamonti@env.ethz.ch)

Abstract. The Asian summer monsoon anticyclone (ASMA) is a major meteorological system of the upper troposphere-lower stratosphere (UTLS) during boreal summer. It is known to contain enhanced in tropospheric trace gases and aerosols, due to rapid lifting from the boundary layer by deep convection and subsequent horizontal confinement. Given its dynamical structure, the ASMA represents an efficient pathway for the transport of pollutants to the global stratosphere. Detailed understanding of the thermal structure and processes in ASMA requires accurate in-situ measurements. Within the StratoClim project we performed state-of-the-art balloon-borne measurements of temperature, water vapor, ozone and aerosol backscatter from two stations at the southern slopes of the Himalayas. In total 63 balloon soundings were conducted during two extensive monsoon-season campaigns, in August 2016 in Nainital, India (NT16_{AUG}) and July-August 2017 in Dhulikhel, Nepal (DK17), and one shorter post-monsoon campaign in Nainital in November 2016 (NT16_{NOV}). These measurements provide unprecedented insights into the UTLS thermal structure, the vertical distributions of water vapor, ozone and aerosols, cirrus cloud properties and interannual variability in ASMA. Here we provide an overview of all the data collected during the three campaign periods, with focus on the UTLS region and the monsoon season. We analyze the vertical structure of ASMA in terms of significant levels and layers, identified from the temperature and potential temperature lapse rates and Lagrangian backward trajectories, providing a framework for relating the measurements to local thermodynamic properties and the large-scale anticyclonic flow. Both the monsoon-season campaigns show evidence of deep convection and confinement extending up to 1.5-2 km above the

Deleted: 9

Deleted: ö

Deleted: 9

Deleted: King Abdullah University of Science and Technology (KAUST), Thuwal, Saudi Arabia

Deleted: be enriched

Deleted: offers

Deleted: very

Deleted: structure and processes

Deleted: Here we present

Deleted: conducted within the StratoClim project

Deleted: we performed

Deleted: main

Deleted: brief

Deleted: ASMA

Deleted: and its relations

Deleted: to

Deleted: To study the structure of the UTLS during the monsoon season, we adopt the thermal definition of tropical tropopause layer (TTL), and define the region of altitudes between the lapse rate minimum (LRM) and the cold-point tropopause (CPT) as the Asian Tropopause Transition Layer (ATTL). Further, based on air mass trajectories, we define the Top of Confinement (TOC) level of ASMA, which divides the lower stratosphere (LS) into a Confined LS (CLS), below the TOC and above the CPT, and a Free LS (FLS), above the TOC.

cold-point tropopause (CPT), yielding a body of air with high water vapor and low ozone which is prone to be lifted further and mixed into the free stratosphere. Enhanced aerosol backscatter also reveals the signature of the Asian tropopause aerosol layer (ATAL) over the same region of altitudes. The Dhulikhel 2017 campaign was characterized by an on average 5 K colder CPT than in Nainital 2016 and a local water vapor maximum in the confined lower stratosphere, about 1 km above the CPT.

Data assessment and modeling studies are currently ongoing with the aim to fully explore this dataset and its implications with respect to stratospheric moistening via the ASMA system and related processes.

1. Introduction

Large-scale deep convection associated with the Asian summer monsoon (ASM) during boreal summer induces a strong and persistent anticyclonic vortex in the upper troposphere - lower stratosphere (UTLS), known as ASM anticyclone (ASMA) (e.g. Hoskins and Rodwell, 1995) or, previously, as Tibetan high (e.g. Krishnamurti and Bhalme, 1976). The ASMA is confined by the subtropical westerly jet stream to the north (40-45°N) and the equatorial easterly jet stream to the south (10-15°N), and spans roughly one third of the northern hemisphere's longitudes (20-140°E). Its geographic center is above the Tibetan plateau and the altitude of maximum strength of the anticyclonic circulation is around the local tropopause (17-18 km), which is the highest worldwide during the ASM season (Dethof et al., 1999; Bian et al., 2012; Garny and Randel, 2016; Ploeger et al., 2015; Pan et al., 2016). The ASMA is subject to strong dynamical variability, oscillations and eddy shedding (Randel and Park, 2006; Yan et al., 2012; Garny and Randel, 2013; Vogel et al., 2014; Nützel et al., 2016).

From satellite measurements, the ASMA is known to be enriched in tropospheric trace species and pollutants, including water vapor, carbon monoxide, methane, hydrogen cyanide, peroxyacetyl nitrate (Randel et al., 2001; 2010; Park et al., 2004; 2007; 2008; Fadnavis et al., 2014; Ungermann et al., 2016), and aerosols, forming the Asian tropopause aerosol layer (ATAL) (Vernier et al., 2011; 2015; Thomason and Vernier, 2013). This is due to persistent deep convection over heavily polluted regions, such as the Indian subcontinent and south-east Asia, lifting pollutants from the boundary layer to the upper troposphere (UT), where the anticyclonic winds keep the air masses horizontally confined. The unique dynamical structure of the ASMA, with tropopause located at higher potential temperature than all its surroundings ($\theta > 380$ K), provides a potentially very efficient pathway for the transport of these pollutants into the lower stratosphere (LS). Transport across the tropopause can occur either vertically across the tropopause, by radiative-driven slow ascent (e.g. Garny and Randel, 2016) or overshooting convection (Fu et al., 2006) ("chimney model"), or adiabatically across the horizontal boundaries of ASMA, hence bypassing the cold-point tropopause ("blower model") (Pan et al., 2016). Lagrangian trajectory calculations suggest that about half of the air mass in ASMA enters the stratosphere by the end of the ASM season (Garny and Randel, 2016), yet which transport pathway is the most effective is currently debated (e.g. Orbe et al., 2015; Garny and Randel, 2016; Pan et al., 2016; Ploeger et al., 2017).

Lagrangian trajectories were also used to investigate the origin of the air masses in ASMA (Bergman et al., 2013; Vogel et al., 2015), although this approach is limited by the convective nature of the transport. Nevertheless, these studies are consistent with satellite observations (Fu et al., 2006), regional weather forecasting (Heath and Fuelberg, 2014) and global atmospheric

Deleted: Using these thermodynamically-significant boundaries, our analysis reveals that the composition of the UTLS is affected by deep convection up to altitudes 1.5-2 km above the CPT due to the horizontal confinement effect of ASMA. This is shown by enhanced water vapor mixing ratios in the Confined LS compared to background stratospheric values in the Free LS, observed in both NT16_{AUG} (+0.5 ppmv) and DK17 (+0.75 ppmv), and by e

Deleted: extending into the Confined LS, as observed in NT16_{AUG}

Deleted: The CPT was 600 m higher in altitude and 5 K colder in DK17 compared to NT16_{AUG} and strong ozone depletion was found in the ATTL and CLS in DK17, suggesting stronger convective activity during DK17 compared to NT16_{AUG}. An isolated water vapor maximum in the Confined LS

Deleted: was also found in DK17, which we argue is due to overshooting convection hydrating the CLS. These evidence show that the vertical distributions and variability of water vapor, ozone and aerosols in the Asian UTLS are controlled by the top height of the anticyclonic confinement in ASMA, rather than by CPT height as in the conventional understanding of TTL, and suggest that the ASMA contributes to moistening the global stratosphere and to increase its aerosol burden.

Deleted: Park et al., 2007

Deleted: between the eastern Mediterranean Sea and the western Pacific Ocean

Deleted: influencing its areal extent, location and strength,

Deleted: The transport

Deleted: isentropically

Deleted: yet

circulation models (Fadnavis et al., 2013; Pan et al., 2016) in indicating the region of the southern slopes of the Himalayas (i.e. approximately latitudes 25-35°N south of the Tibetan plateau) as a hot-spot for the transport of boundary layer pollutants to the ASMA. Considering the recent rapid increase of pollutant emissions from India (e.g. Krotkov et al., 2016) it is crucial for global chemistry climate models to properly represent the ASMA dynamics, thermodynamic structure and processes.

Up to date, most of the observational evidence regarding the chemical composition of the Asian UTLS is derived from satellite measurements, providing information with good regional and temporal coverage, but with limited vertical resolution. Highly vertically-resolved datasets in the UTLS are important to understand the physical boundaries that control the vertical distribution of chemical species, and microphysical processes like the nucleation of cirrus clouds and aerosols. This requires accurate in-situ measurements in ASMA. Aircraft measurements are available from dedicated campaigns (e.g. Gottschaldt et al., 2018) or civil aviation-based observational networks (e.g. Rauthe-Schöch et al., 2016), yet these are either sparse in space and time, or limited by the relatively low cruising altitude of passenger aircrafts (10-12 km). Balloon-borne measurements are particularly suited for the investigation of the UTLS, and balloon campaigns dedicated to the study of the ASMA and ATAL increased in frequency over the last decade (e.g. Bian et al., 2012; Vernier et al., 2018; this work).

In this article we present and discuss the data collected by the StratoClim balloon campaigns, carried out from two sites at the southern slopes of the Himalayas through the years 2016 and 2017. State-of-the-art instruments were used to measure vertical profiles of temperature, water vapor, ozone and aerosol backscatter, from the surface to the middle stratosphere. Here we first provide an overview of all measurements, showing mean profiles and their standard deviation ranges of natural variability for the different campaign periods, and then focus on analyzing the thermodynamic structure of the UTLS during the ASM season and how it relates with the distributions and variability of water vapor, ozone and aerosols. One aim of this work is also to pave the way for ongoing more targeted modeling and intercomparison studies within StratoClim and other activities.

2. Campaign description, instruments and data processing

The measurements were performed in Nainital, Uttarakhand, India (29.35°N, 79.46°E: NT) and Dhulikhel, Nepal (27.62°N, 85.54°E: DK), hosted respectively by the Aryabhata Research Institute of Observational Sciences (ARIES) and Kathmandu University (KU). Both sites are located at the southern slopes of the Himalayan mountain range, at elevations of 1820 m (NT) and 1530 m (DK) above sea level. In this region, the terrain elevation increases steeply from sea-level heights of the Indo-Gangetic plane to the south, to elevations above 3000 m of the Tibetan plateau to the north, and strong orographic forcing induces persistent deep convection and heavy rainfall during the monsoon season (Vellore et al., 2016).

The measurements were conducted during three distinct periods of time, including two extensive monsoon campaigns, in NT in 2016 (2-31 August, 30 balloon soundings: NT16_{AUG}) and in DK in 2017 (30 July - 12 August, 28 balloon soundings: DK17), and one shorter post-monsoon campaign in NT (2-8 November 2016, 5 balloon soundings: NT16_{NOV}) (note that a list of the main acronyms used in this paper, including the abbreviations of stations and campaign periods, is given in Table 1). The

Deleted: and south-east Asia, due to their fast economic growth,

Deleted: vertical resolution is

Deleted: a notoriously hardly accessible region such as the UTLS, and balloon-borne measurements are particularly suited for this aim

Deleted: In total 63 balloon soundings were performed in Nainital (India) and Dhulikhel (Nepal) during three distinct periods of time, including two main monsoon-season campaigns (August 2016 in Nainital and July-August 2017 in Dhulikhel), and one brief post-monsoon campaign (November 2016 in Nainital).

Deleted: with

Deleted: main

frequency of the soundings and the composition of the payloads varied depending on meteorological conditions and on operational constraints. ~~Various logistic limitations affected our DK17 campaign, resulting in a reduced measurement schedule~~ (most notably, the number of backscatter measurements was limited: see Table 1). Nevertheless, important scientific data were collected. The DK17 campaign took place simultaneously with the StratoClim aircraft campaign, based in Kathmandu Airport (Nepal), which performed 8 scientific flights with the high-altitude Geophysica-M55 research aircraft.

All soundings employed meteorological latex balloons (Totex, Japan) filled with hydrogen gas in order to ascend at a rate of about 5 m/s. Maximum burst altitude of these balloons is around 35 km, and more than 70% of our soundings reached at least 30 km (see Table S1 in supplementary material). A standard meteorological radiosonde was used to host additional instruments through its XDATA interface (Oelsner and Tietz, 2017), and to transmit the data of all instruments to the ground station at 1 Hz frequency. In particular, we used RS41-SGP (Vaisala, Finland) radiosondes (Vaisala, 2017), and the DigiCora MW41 sounding system (Vaisala, Finland) as ground station (Vaisala, 2014). Additional instruments employed were: Electrochemical Concentration Cell (ECC, manufacturer: En-Sci, USA) (Komhyr, 1969) for ozone (O_3) mixing ratio, Cryogenic Frost-point Hygrometer (CFH, En-Sci, USA) (Vömel et al., 2007; 2016) for water vapor (H_2O) mixing ratio, and Compact Optical Backscatter Aerosol Detector (COBALD, MyLab, Switzerland) for aerosol backscatter.

For the pressure (p) and temperature (T) measurements that we analyze in this work, uncertainties of RS41-SGP (hereafter: RS41) given by the manufacturer are 0.6/1 hPa (at pressures lower/higher than 100 hPa) and 0.3/0.4 K (at altitudes lower/higher than 16 km), respectively. The performances of ECC sondes have been assessed by many studies (e.g. Smit et al., 2007), and uncertainties are estimated as 5-10% in terms of O_3 partial pressure. CFH is a frost-point hygrometer based on the chilled-mirror principle with uncertainty on H_2O mixing ratio lower than 10% up to 28 km altitude (Vömel et al., 2007). ECC and CFH are regularly deployed in the ASM region since 2009 (Bian et al., 2012). COBALD is a detector for aerosol backscatter measurements at optical wavelengths of 455 nm (blue visible) and 940 nm (infrared) developed at ETH Zürich, downscaling the original backscatter sonde by Rosen and Kjome (1991) in weight and size. COBALD is able to detect cirrus clouds (e.g. Brabec et al., 2012) as well as aerosol layers, such as ATAL (Vernier et al., 2015). In addition, one RS92-SGP radiosonde (Vaisala, Finland) was added to almost all payloads for an intercomparison with the performances of RS41 (not discussed in this paper). Finally, we note that for logistical constraints, the first two soundings in NT16_{AUG} employed iMet-1-RSB radiosondes (InterMet, USA) (InterMet, 2006), offering the XDATA interface (Wendell and Jordan, 2016), instead of RS41, and SkySonde version 1.9 (Jordan and Hall, 2016) as data acquisition software.

In this study, we use the pressure measured by RS41 as the main vertical coordinate for all instruments. All variables are binned in pressure intervals of 1 hPa for $p > 300$ hPa, and 0.5 hPa for $p < 300$ hPa, yielding an improved signal-to-noise ratio and a dataset with consistent vertical levels. This binning corresponds to a vertical resolution of approximately 25 m in the UTLS. A quality check is performed for all instruments based on interpretation of their house-keeping data, and data points showing anomalous behavior are rejected (note that the number of malfunctioning events per instruments are noted in brackets in Table 1). In this context, ~~the contamination of CFH measurements deserves a special mention, as this effect~~ was observed

Deleted: In the past, attempts of conducting field campaigns in the ASM region were often hindered by operational and

Deleted: ,

Deleted: which also

Moved down [1]: The number of deployments of each instrument during the different campaign periods are summarized in Table 1. A list of all the 63 soundings with date and time of launch, payload description, burst altitude and other notes is given in Table S1 in supplementary material.

Deleted: CFH deserves a special mention, since a behavior we named “CFH contamination”

in a significant number of cases. This consists in the drift towards ~~high~~ frost-point temperatures ~~in the stratosphere, corresponding to~~ water vapor mixing ratios ~~exceeding physical constraints~~ (see Figure S1 in supplementary material) which we attribute to the deposition of supercooled water droplets onto the inner walls of the instrument's inlet tube while passing through mixed-phase clouds. This hypothesis is currently subject of a dedicated modeling study. To avoid such instrumental artifact, for the analysis in this paper we do not accept H₂O mixing ratio measurements higher than 10 ppmv in the stratosphere, which are unrealistic, as well as all measurements at pressures below 20 hPa (see Section 3.3). Ice saturation (S_{ice}), i.e. relative humidity with respect to ice, is calculated using the frost-point temperature measured by CFH, air temperature by RS41, and the parameterization for saturation vapor pressure over ice by Murphy and Koop (2005). The COBALD data are expressed as backscatter ratio (BSR), i.e. the ratio of the total-to-molecular backscatter coefficient. This is calculated by dividing the total measured signal to its molecular contribution, which is computed from the atmospheric extinction according to Bucholtz (1995), and using air density derived from the measurements of temperature and pressure (see Cirisian et al., 2014). Uncertainty on COBALD BSR as inferred by this technique is estimated around 5% (Vernier et al., 2015).

~~The number of deployments of each instrument during the different campaign periods are summarized in Table 2. A full list of all the 63 soundings with date and time of launch, payload description, burst altitude and other notes is given in Table S1 in supplementary material.~~ Note that for conversion of pressure to geometric altitude (z), mean profiles of p vs. z measured by RS41 are shown in Figure S2 in supplementary material.

3. Data overview

Figure 1 shows mean profiles and standard deviations of temperature, H₂O mixing ratio and O₃ mixing ratio calculated from all measurements performed during the three campaign periods, namely NT16_{AUG} (blue), NT16_{NOV} (green) and DK17 (red).

Panels a-c show the entire measured profiles, while Panels d-f show zooms into the UTLS region. In this section we briefly discuss their main features. Aerosol backscatter measurements will be discussed in Section 6.

In the troposphere ~~average H₂O mixing ratios differ by~~ up to a factor of 40 in the lower troposphere between the dry (November) and the ASM season (July–August). Massive latent heat release by condensation during the wet period, in contrast to dry conditions in winter, is reflected in different lower tropospheric lapse rates for the two seasons, with about 5.5 K/km in July–August, and 8 K/km in November. ~~This is consistent with the meridional shift of the intertropical convergence zone (ITCZ) and the associated deep convection patterns in the Asian sector, reaching about 30°N in boreal summer (Lawrence and Lelieveld, 2010).~~ Lower tropospheric O₃ in NT16_{AUG} compared to NT16_{NOV} is likely due to enhanced washout of ozone precursor gases during the wet season. Higher O₃ in the lower troposphere in NT16_{AUG} vs. DK17 might be due to photochemical smog transport from the New Delhi urban area and the highly populated Indo-Gangetic plane (e.g. Kumar et al., 2010).

The structure of the tropopause region is very different during the three measurement periods. In contrast to the sharp cold-point tropopause (CPT) of the ASM season, ~~the~~ November ~~measurements show~~ an almost isothermal layer above the lapse-rate tropopause (LRT, defined according to the World Meteorological Organization: WMO, 1957), ~~such that~~, in NT16_{AUG} and

Deleted: too

Deleted: hence too high

Deleted: in the stratosphere

Moved (insertion) [1]

Deleted: 1

Deleted: Finally,

Deleted: n

Commented [BS1]: Subsections 3.1, 3.2, 3.3 eliminated

Deleted: General

Deleted: of the data

Deleted: Note that for improved recognition, we keep this color coding also in subsequent figures.

Deleted: 3.1 Troposphere ¶

Deleted: , seasonal variability of water vapor mixing ratio is the most evident feature, with differences

Deleted: (close to the moist adiabat)

Deleted: (close to the dry adiabat)

Deleted: Additionally, in the upper troposphere, the same feature is likely also related to stronger convective activity occurring during DK17 compared to NT16_{AUG} (discussed in Section 5.2).

Deleted: 3.2 Tropopause region¶

Deleted: typical of the tropics, the tropopause structure in

Deleted: has more similarity to that in the mid-latitudes, with

Deleted:)

Deleted: (

Deleted: As a consequence

DK17 the LRT coincides with the CPT, whereas in NT16_{NOV} the average LRT and CPT are about 2.5 km apart. Seasonal variations of the LRT-CPT separation are consistent with Munchak and Pan (2014) and related to varying meridional position of the jet stream (see Section 4.1). Interestingly, comparing the two ASM seasons datasets also reveals significant differences. The average CPT is 10 hPa higher (88 vs. 97.5 hPa, corresponding to about 600 m in altitude) and 5 K colder (-81.7 vs. -76.8 °C) in DK17 compared to NT16_{AUG}. Water vapor in the UTLS is minimum in NT16_{NOV}, with mixing ratios around 2.5 ppmv above the LRT. During the ASM, UTLS H₂O is higher, but different vertical distributions are observed. In NT16_{AUG}, H₂O mixing ratio decreases monotonically with altitude, with mean value of 6.8 ppmv at the CPT. In DK17, H₂O mixing ratio shows a minimum at the CPT (3.5 ppmv), and a local maximum above it (6 ppmv). Mean altitude, pressure, potential temperature and temperature of the LRT and CPT for the three campaign periods are summarized in Table 2.

Lower stratospheric temperatures (20-60 hPa) differ by about 2-4 K between November and July-August, which is consistent with the climatological annual cycle of stratospheric temperature (Randel et al., 2003). Stratospheric H₂O mixing ratios are in the range of 4-6 ppmv up to 20 hPa, with a slight increase with altitude due to oxidation of methane. Above approximately 20 hPa (27 km), all CFH measurements show an unrealistic increase in H₂O mixing ratio, which is a measurement artifact. At such high altitudes and low air densities, outgassing from the balloon skin and the payload train can play a significant role in contaminating the humidity measurements (Kräuchi et al., 2016). Hence, water vapor data in this range will not be considered in this analysis. Differences in stratospheric ozone between NT16_{AUG} and DK17 are likely due to interannual variability.

4. Meteorological overview

For relating the measurements to the large-scale atmospheric flow, here we analyze meteorological data from the European Center for Medium-range Weather Forecast (ECMWF) for the three campaign periods.

4.1 Seasonal variability

Figure 2 illustrates the seasonal variability of the meteorological systems above the southern slopes of the Himalayas during NT16_{AUG} (top row), NT16_{NOV} (center), and DK17 (bottom row). The left column (panels a, c, e) shows latitude-pressure cross sections of potential vorticity (PV), potential temperature and total wind speed for NT (longitude 80° N, panels a, c) and DK (longitude 85°E, Panel e) from ECMWF analysis data averaged over the time of the respective measurement periods. The right column (panels d, b, f) shows average geopotential height at 100 hPa for the three measurement periods from ECMWF analysis data, superimposed with 2-weeks backward air mass trajectories initialized at 100 hPa at the time of each sounding during the three campaign periods. Trajectories are calculated by the Lagrangian Analysis Tool (LAGRANTO) (Wernli and Davies, 1997), based on ERA-Interim re-analysis wind fields, and color-coded with pressure.

During the NT16_{AUG} and DK17 campaigns (panels a-b, e-f), our stations are located inside the ASMA vortex. The continental-scale anticyclonic motion is confined by the subtropical westerly jet stream north (40-45°N), and the equatorial easterly jet to

Deleted: was found at 108 hPa

Deleted: the

Deleted: at 69.5 hPa, i.e.

Deleted: in the LS

Deleted: Lower O₃ in the tropopause region during the ASM than in November is likely related to the monsoonal deep convection, transporting ozone-poor air from the boundary layer to the UT.

Deleted: 3.3 Stratosphere ¶

Deleted: the corresponding dry conditions and

Deleted: analysis

Deleted: focusing on the UTLS region

Deleted: , in terms of latitude-pressure cross-sections (left column) and air mass backward trajectories (right column). ¶ In particular, Figure 2 (

Deleted: (θ),

Deleted: zonal

Deleted: and ice water content,

Deleted: on selected days.

Deleted: ASM season (Panels a, e),

the south (10-15°N). Both NT and DK, during their respective measurement periods, are found in the region of average geopotential height exceeding 16.8 km at 100 hPa, which is the highest in ASMA. Backward trajectories show that the UTLS flow at the southern slopes of the Himalayas is mainly easterly, following the southern branch of the ASMA, and transporting air masses which were confined inside the anticyclone already for several days. During the last 2 weeks prior to their respective measurement, the air masses sampled at 100 hPa during our campaigns undergo net diabatic ascent, at an average rate of 0.7 K/day and 0.4 K/day (in isentropic coordinates) for NT16_{AUG} and DK17, respectively. The equatorial easterly jet was slightly stronger and extended further north during the ASM season 2017 (panel e) compared to 2016 (a) which is also reflected by the corresponding backward trajectories (b, f). North of the subtropical westerly jet, the dynamical tropopause (corresponding to PV = 3-4 PVU in this region and season: Kunz et al., 2011).

After the end of the monsoon season, the subtropical westerly jet migrates southward to 30-35°N and intensifies in strength. Therefore, during the post-monsoon campaign NT16_{NOV} (panels c-d), our station is located below the jet and the associated tropopause break, resulting in the large LRT-CPT separation discussed in Section 3. This is consistent with wind speed and direction measurements by RS41 shown in Figure S3 in supplementary material. We also note that, the large standard deviation of temperature in the tropopause region in NT16_{NOV} (Figure 1d) is likely related to varying meridional position of the jet stream during the measurement period.

The dynamical features discussed above are consistent with the seasonal variations of the ITCZ, the jet streams and the ASM system in general, which are extensively discussed in previous literature, e.g. Lawrence and Lielveld (2010), Munchak and Pan (2014), Ploeger et al. (2015), Garny and Randel (2016), Pan et al. (2016).

4.2 Interannual and regional variability

To assess whether the differences between the observations in NT16_{AUG} and DK17 are caused mainly by geographic difference, and associated different mesoscale weather features, or by interannual variability between the ASM 2016 and 2017 seasons, in Figure 3 we examine time series of UTLS temperature and H₂O mixing ratio from ECMWF analysis data for both stations and both campaign periods.

In August 2016 (Panels a-d), the UTLS was relatively warm at both locations, with CPT temperatures rarely below -80°C and DK slightly colder than NT (0.4 K on average at 100 hPa), and H₂O mixing ratio did never decrease below 4.5 ppmv at both sites. The same day-to-day variability features are visible at both locations with a time shift of about 6-12 h, which is consistent with DK being systematically upstream of NT along the southern branch of the ASMA, and a wind speed of around 20 m/s in the UTLS. In July-August 2017 (Panels e-h), T and H₂O values and features are similar to 2016 until 3 August. Then, a period characterized by extremely cold and dry tropopause starts in both NT and DK, peaking between 7-10 August with CPT temperatures colder than -83°C and H₂O mixing ratios lower than 3 ppmv. The minima are slightly more pronounced in DK than in NT but are correlated in time, suggesting that these features are related to a large-scale cooling and drying pattern occurring in the ASMA. Interestingly, we also note that a layer of high H₂O rises to high altitudes (70-85 hPa) after 3 August (Panel f),

Deleted: limits the ASMA on its northern flank around 40-45°N, and marks the border between a "tropical regime" to the south, including the ASMA, and the mid-latitudes to the north. The dynamical tropopause (i.e. the PV = 2 PVU surface) is found at about 100 hPa inside the ASMA, while n

Deleted: jet it decreases steeply with altitude.

Deleted: Hence, in November (Panel c), NT is located at the boundary between the tropical and mid-latitude regimes, i.e.

Moved (insertion) [2]

Deleted: quasi-isothermal lapse rate between the LRT and CPT discussed in Section 3.2. Additionally

Deleted: (see Figure 1, Panel d).

Moved up [2]: This is consistent with wind speed and direction measurements by RS41 shown in Figure S3 in supplementary material.

Deleted: Figure 2 (right column) shows 2-weeks backward air mass trajectories calculated by the Lagrangian Analysis Tool (LAGRANTO) (Wernli and Davies, 1997), based on ERA-Interim re-analysis wind fields, and initialized at 100 hPa at the time of each sounding. During the ASM season (Panels b, f) the UTLS flow at the southern slopes of the Himalayas is easterly and follows the southern branch of the ASMA, transporting air which has been circulating around the anticyclone already for several days. In contrast, in November (Panel d), the UTLS winds are westerly and follow the subtropical jet stream, carrying air from above the Saharan desert and air masses deflected from the equatorial easterlies. This is consistent with wind speed and direction measurements by RS41 shown in Figure S3 in supplementary material. ¶

Deleted: clearly

forming the local maximum above the CPT which we also find in our DK17 measurements (Figure 1, Panel e). This feature is remarkable and not in accordance with more typical climatological conditions observed during NT16_{AUG}.

Based on Figure 3, we argue that the differences between the NT16_{AUG} and DK17 datasets are not due to local meteorological effects, which appear to have negligible impact on the UTLS temperature and water vapor at the two measurement sites.

Rather, these differences are to be attributed to interannual variability, and in particular to to a period of anomalously cold and dry UTLS at the southern slopes of the Himalayas, occurring after 3 August 2017 and persisting on a large scale.

5. UTLS structure during the ASM season

In this section we focus on analyzing the UTLS structure of the NT16_{AUG} and DK17 measurements. The NT16_{NOV} measurements will be discussed again in Section 6.

5.1 Asian tropopause transition layer (ATTL)

In the tropics, the thermodynamic transition between the troposphere and the stratosphere occurs over a layer of several kilometers in thickness, termed tropical tropopause layer (TTL). This layer is influenced by both upper tropospheric and lower stratospheric processes, and its properties control water vapor transport through the tropopause (e.g. Fueglistaler et al., 2009; Randel and Jensen, 2013). Amongst several different definitions of TTL used in the literature, reviewed by Pan et al. (2014),

Gottelman and de F. Forster (2002) identify the TTL boundaries based on the temperature and potential temperature lapse rates only, which is particularly suited for balloon-borne measurements. In their definition, the upper boundary of the TTL is the CPT, and the lower boundary the lapse rate minimum (LRM) level, i.e. the point in altitude where the change of potential temperature (θ) with altitude (z) is minimum. This defines the TTL as the layer in which the temperature lapse rate switches from convectively-dominated in the troposphere (small $d\theta/dz$, low stability), to radiatively-controlled in the stratosphere (high $d\theta/dz$, high stability) (Gottelman and de F. Forster, 2002). In addition, the LRM coincides with the mean convective outflow level (Gottelman and de F. Forster, 2002; Vömel et al. 2002; Paulik and Birner, 2012). Given the similarity between the Asian tropopause region during the ASM season and that of the tropics, here we adopt this definition of TTL to study the thermal structure of our NT16_{AUG} and DK17 datasets. However, being our measurement sites not tropical in a geographic sense, we refer to the TTL in this region and season as the Asian tropopause transition layer (ATTL).

Figure 4 shows mean profiles and standard deviations of $d\theta/dz$ as a function of pressure for the two ASM season datasets. The average LRM is also found at lower pressure in DK17 compared to NT16_{AUG}, corresponding to to roughly 400 m altitude difference, and the minimum in $d\theta/dz$ of DK17 is more pronounced (1.5 vs. 2 K/km). This suggests that, on average, convection reached higher altitudes in the ASM 2017 compared to the year 2016, at least during the time of our measurements. The average ATTL boundaries in terms of pressure (potential temperature) are 180-97.5 hPa (360-382 K) for NT16_{AUG}, and 169.5-88 hPa (362.5-383.5 K) for DK17 (see Table 3: note that the data are binned with respect to pressure and the given potential

Deleted: To quantify this resemblance, Figure 4 shows mean measured profiles of temperature (Panels a-b) and H₂O mix [...]

Deleted: In summary, here

Deleted: anomalously strong convective activity

Deleted: in the ASM

Moved down [3]: 4.3 Horizontal confinement in ASMA

Deleted: Thermodynamic structure

Deleted: In the Brewer-Dobson circulation, tropical CPT [...]

Deleted: does not occur instantaneously, but

Deleted:), and the properties of the TTL rather than CPT [...]

Deleted: Highwood and Hoskins, 1998; Holton and Gettelman [...]

Deleted: As discussed

Deleted: different definitions of TTL are used in the literature [...]

Deleted: profiles and derived

Deleted: our

Deleted: Using this definition of TTL, Pan et al. (2014) [...]

Deleted: (see Sections 3.2, 4.1)

Deleted: the UTLS in

Deleted: strict

Deleted: (NT and DK are at latitudes 27-30°N)

Deleted: , or Asian TTL

Deleted: 6

Deleted: T , θ and

Deleted: As already noted in Section 3.2, the average CPT [...]

Deleted: higher altitude by roughly 10 hPa

Deleted: (Panel c)

Deleted: a 2.5 K difference near the 360 K isentropic level

Deleted: Higher LRM and higher and colder CPT in DK17

Deleted: prior and

Deleted: exact

Deleted: and average

Deleted: and

Deleted: ,

Deleted: 2

temperature values are the average θ in the pressure levels where the LRM and CPT occur). We also observe that, due to the colder temperatures, the isentropic levels in DK17 are shifted to lower pressures compared to NT16_{AUG} (see Figure S4 in supplementary material), so that the large altitude difference between the two LRM and CPTs in NT16_{AUG} compared to DK17 (400-600 m) becomes small in isentropic coordinates (1.5-2 K).

5.2 Confined lower stratosphere (CLS)

Since the anticyclonic circulation extends up to above the CPT, it is important for interpreting the observed vertical gradients of chemical species and aerosols to quantify the vertical extent of ASMA in the lower stratosphere. Here we estimate the top of the horizontal confinement effect of ASMA during the NT16_{AUG} and DK17 campaign periods by means of air mass trajectories. For this, we consider 2-weeks LAGRANTO backward trajectories initialized at 5 hPa intervals between 40 and 150 hPa at the time of each balloon sounding in NT16_{AUG} and DK17 (i.e. same as shown in Figures 2b, 2f for 100 hPa) and 6 h before and 6 h after each sounding, using ERA-Interim re-analysis wind fields. For each pressure level, we calculate the “confined fraction” of trajectories, defined as the fraction of trajectories which were already located inside the anticyclone 2 weeks before the measurements. For this purpose, based on the average geopotential height fields shown in Figures 2, we approximate the ASMA area as the box of 10-50°N latitude, 20-140°E longitude (see white dashed rectangle in Figures 2b, 2f).

Figure 5 shows the resulting confined fractions for NT16_{AUG} and DK17 as a function of pressure in Figure 5. In both campaign periods, the confined fraction is high (above 60%) up to 70-80 hPa, while above it sharply decreases to zero. Confinement is higher for DK17 than for NT16_{AUG} throughout the entire UTLS, which is qualitatively consistent with the backward trajectories shown in Figure 2. Based on these curves, we define the top of confinement (TOC) level of ASMA as the level of confined fraction = 50%, corresponding to 73 hPa in NT16_{AUG} and 63.5 hPa in DK17. This level separates altitudes which are affected by horizontal confinement in ASMA (below TOC), from the confinement-free lower stratosphere above the ASMA (above TOC). Note that mean altitude and potential temperature of the TOC levels derived from the balloon measurements are given in Table 3.

Following from the definition of TOC, we further define the confined lower stratosphere (CLS) as the region of altitudes above the CPT and below the TOC. The CLS is the layer of lower stratosphere which is subject to confinement in ASMA, in contrast to the free stratosphere above the anticyclonic vortex (i.e. above TOC). Figure 6 illustrates the vertical structure of the UTLS above the southern slopes of the Himalayas during the ASM season according to the definitions of ATTL and CLS just introduced. In the following of this work, we refer to this framework of thermodynamically-significant levels and layers to discuss the vertical distributions and variability of water vapor, ozone, ice saturation and aerosols in ASMA.

5.3 Water vapor and ozone

To analyze our H₂O and O₃ measurements in relation to the thermodynamic structure of the UTLS, we define for each balloon sounding the altitude relative to the CPT as a new vertical coordinate. Figure 7 shows mean profiles and standard deviations

Deleted: the potential temperature values are the average θ in the pressure levels where the LRM and CPT occur, and the data of individual soundings are not binned with respect to potential temperature

Deleted: We also note that the measured profiles of $d\theta/dz$ and mean LRM levels are in good agreement with ECMWF operational data (Figure 4, Panels c, f).

Commented [BS3]: Section 4.3 moved to Section 5.2

Moved (insertion) [3]

Deleted: Figure 7 highlights the levels and layers used throughout this work (see also the summary in Figure 12 at the end of this paper). Based on the definitions of LRM, CPT and TOC (introduced in Section 4.3), hereafter we will refer to: UT as the region of altitudes below the LRM, Asian TTL (ATTL) as the region between LRM and CPT, Confined LS (...)

Deleted: Horizontal confinement in ASMA

Deleted: In conclusion of the meteorological overview, w (...)

Deleted: calculate

Deleted: with LAGRANTO using ERA-Interim re-analys (...)

Deleted: , Panels

Deleted: then

Deleted: T

Deleted: he ASMA area is

Deleted: d

Deleted: shown by grey

Deleted: lines

Deleted: , Panels b, f

Deleted: T

Deleted: are plotted

Deleted: Therefore,

Deleted: the anticyclonic

Deleted: of

Deleted: the

Deleted: M

Deleted: 2

Deleted: In Sections 5 and 6, we will show that the TOC (...)

Deleted: 2

Deleted: the vertical distributions and variability of tracers

of temperature, H₂O mixing ratio and O₃ mixing ratio in this coordinate system (note that, besides the CPT in black, the average LRM and TOC levels are shown by blue dashed for NT16_{AUG}, and red dashed lines for DK17). Figure 8 shows probability density functions (PDFs) of temperature (left column), H₂O mixing ratio (center) and O₃ mixing ratio (right column) calculated in the free stratosphere (panels a-c), CLS (d-f), ATTL (g-i) and troposphere (j-l) regions, for NT16_{AUG} and DK17. The PDFs of the free stratosphere region are calculated for altitudes between TOC and CPT + 5 km, while the troposphere PDFs between

CPT – 6 km and LRM, i.e. covering the whole range of altitudes (with respect to CPT) as shown in Figure 7. Water vapor mixing ratio in DK17 shows a minimum at the CPT and a local maximum in the CLS (Figure 7b), centered about 1 km above the local CPT (i.e. not the average CPT, but evaluated for each profile individually). The H₂O minimum is conceivably due to unusually high frequency of occurrence of ice clouds near the CPT in DK17, depleting water vapor from the gas phase in favour of the condensed phase, hence resulting in a strongly dehydrated CPT (see Section 5.4). The isolated H₂O maximum in the CLS is consistent with hydration by overshooting convective updrafts, injecting ice crystals above the CPT, which then evaporate and thus release localized “pockets” of moist air. Convective updrafts overshooting the CPT were observed by Corti et al. (2008), and a similar hydration mechanism was hypothesized by Dauhut et al. (2015; 2016).

In both NT16_{AUG} and DK17, the PDFs of H₂O mixing ratio show high water vapor in the CLS (Figure 8e) compared to the free stratosphere (Figure 8b). In particular, the PDFs in the CLS are broad (3-7 ppmv) and skewed towards high values, while the PDFs in the FLS are narrow (3-5 ppmv) and show the expected distribution of background stratospheric H₂O mixing ratios. The high H₂O mixing ratios in the CLS compared in DK17 are obviously related to the previously discussed isolated maximum, yet enhanced frequency of occurrence of high H₂O mixing ratios is also observed in NT16_{AUG} despite no local maximum was found in this dataset. This is consistent with the slow ascent of moist convective outflow air within the confined anticyclone, and in part may reflect the decreasing frequency of overshooting convective tops with altitude in NT16_{AUG}.

Ozone mixing ratio in DK17 shows a minimum slightly above the LRM (Figure 7c), which is characteristic of deep convection, rapidly transporting ozone-poor air from the boundary layer to the convective outflow level (Gettelman and de F. Forster, 2002; Vömel et al. 2002; Paulik and Birner, 2012), suggests that the average age of air, meant as the time elapsed since the last interaction with deep convection, was higher in NT16_{AUG} compared to DK17, such that the O₃ minimum is smeared out by mixing and additional photochemical production (which is enhanced in ASMA due to the enrichment in ozone precursors; Gottschaldt et al., 2018). Higher dilution of the convective signature in NT16_{AUG} vs. DK17 is also consistent with the absence of an H₂O maximum above the CPT in NT16_{AUG} (Figure 7b), and with the high frequency of occurrence of low O₃ mixing ratios in DK17 compared to NT16_{AUG} in the ATTL and CLS (Figures 8f, 8i).

In summary, both the NT16_{AUG} and DK17 datasets show evidence of deep convection extending into the CLS, i.e. up to 1.5-2 km above the CPT. Convective features, such as low O₃ in the ATTL and high H₂O in the CLS, are more pronounced in DK17 than in NT16_{AUG}, indicating that DK17 likely sampled fresh convective outflow more frequently than NT16_{AUG}. This is also consistent with the higher altitude of the LRM in DK17 compared to NT16_{AUG} (Figure 4) and suggests that convective activity at the southern slopes of the Himalayas was more frequent during the ASM season 2017 than in 2016.

Deleted: new ...coordinate system. B... (note that, besides the CPT (...n black dashed line)... the average LRM and TOC levels are shown by blue dashed and dotted lines, respectively (blue

Moved (insertion) [4]

Deleted: FLS...ree stratosphere (P...anels a-c), CLS (Panels d-f), ATTL (Panels ...-i) and UT...roposphere (Panels

Deleted: isolated ...aximum in the Confined ...S (Figure 7bPanel b... centered about 1 km above the local CPT (i.e. not the average CPT, but evaluated for each profile individually). The H₂O minimum at the CPT ...s conceivably due to unusually high frequency of occurrence of ice clouds near the CPT in DK17 (see Ice saturation discussion in Section 5.3)... which ...eplete...ng water vapor from the gas phase in favour of the condensed phase, hence resulting in a strongly dehydrated CPT (see Section 5.4). The isolated H₂O maximum in the CLS is consistent with hydration by likely due to ...ershooting convective updrafts, injecting ice crystals directly above the CPT, which then evaporate at higher levels ...nd and thus release localized “pockets” of moist air.hence hydrate the CLS

Moved down [5]: A minimum in O₃ mixing ratio slightly above the LRM is found in DK17 (Panel c), which is characteristic of very strong convection, quickly transporting ozone-poor air from the boundary layer to the TTL (Gettelman and de F. Forster, 2002; Vömel et al. 2002; Paulik and Birner, 2012). The absence of this feature in NT16_{AUG} corroborates the statement that convection was stronger during DK17 compared to the ASM 2016 season.¶

Deleted: A minimum in O₃ mixing ratio slightly above the above the LRM is found in DK17 (Panel c), which is characteristic of very strong convection, quickly transporting ozone-poor air from the boundary layer to the TTL (Gettelman and de F. Forster, 2002; Vömel et al. 2002; Paulik and Birner,

Moved up [4]: Figure 8 shows probability density functions (PDFs) of temperature (left column), H₂O mixing ratio (center) and O₃ mixing ratio (right column) calculated in the FLS

Deleted: datasets... the PDFs of H₂O mixing ratio show enhanced ...igh water vapor in the CLS (Figure 8e) compared to the free stratosphere (Figure 8b)Confined LS (Panel e) compared to the Free LS (Panel b)... In particular, the PDFs in

Deleted: We argue that this enhancement is due to the anticyclonic confinement effect of ASMA, which keeps the moist convective outflow horizontally confined and thereby in-

Moved (insertion) [5]

Deleted: A minimum in O₃ mixing ratio ...lightly above the LRM (Figure 7c) is found in DK17 (Panel c)... which is characteristic of very strong...eep convection, quickly...apidly transporting ozone-poor air from the boundary layer to the

Transport to the CLS is likely a combination of different processes, including overshooting convection, slow diabatic ascent, as well as adiabatic transport from regions with higher CPT potential temperature in ASMA (discussed in Section 7). Although we do not quantitatively evaluate these processes, we argue that the horizontal confinement effect of ASMA plays an important role in shaping the vertical distributions of H₂O and O₃ above the CPT, by keeping the moist convective outflow horizontally confined (while it continues to rise slowly) and thereby increasing the frequency of occurrence of air parcels with high H₂O and low O₃ above the CPT. This is supported by the fact that differences in H₂O and O₃ between NT16_{AUG} and DK17 vanish in the free stratosphere (Figure 8a-c), which is in agreement with our trajectory-based definition of TOC. Further analysis will be required to disentangle the relevance of the different transport processes mentioned above in moistening the CLS.

5.4 Ice saturation

Figure 9 shows mean profiles and standard deviations of ice saturation (panel a) and histograms of supersaturated fraction (b), as a function of altitude relative to CPT, and PDFs of ice saturation calculated for the troposphere, ATTL and CLS regions (c-e). As a result of significantly colder temperatures (see Figure 7a), much higher and more persistent ice saturations were measured in DK17 than in NT16_{AUG} throughout the entire ATTL. In both datasets, ice saturation is higher in the ATTL compared to the UT, and in DK17 it shows a pronounced maximum with average supersaturated conditions (i.e. more than 50% of the measurements reach $S_{ice} > 1$) in the 1.5 km directly below the CPT. In contrast, the supersaturated fraction is 10-15% in NT16_{AUG} over the same range of altitude. The ATTL ice saturations and supersaturated fractions of NT16_{AUG} are comparable with previous measurements in Lhasa and Kunming, China during 2009-2012 (Bian et al., 2012) while the measurements in DK17 range significantly higher. This suggests that the frequency of occurrence of cirrus clouds in the ASM season 2017 was unusually high, which is likely the reason for the H₂O minimum at the CPT observed in DK17 (Figure 7b). Interestingly, we also note that ice supersaturations in DK17 extend frequently into the CLS, with about 30% supersaturated fraction in the first 500 m above the CPT (Figures 9b, 9c). This implies that, in overshooting convective updrafts, ice crystals can regularly penetrate the CPT as condensed phase (e.g. see Figure 10f) and hence efficiently hydrate the CLS.

6. Aerosol and cloud backscatter

In this section, we analyze the aerosol and cloud backscatter measurements by COBALD, which have not been discussed so far. COBALD was originally designed and used to investigate the properties of ice cloud, including cirrus (e.g. Brabec et al., 2012; Cirisian et al., 2014) and polar stratospheric clouds (e.g. Engel et al., 2014), yet recent measurements from Lhasa, China were also used for in-situ detection of the ATAL aerosols (Vernier et al., 2015; 2018). Here, we address both aspects. Since the BSR of aerosol droplets is 1-2 orders of magnitude smaller than that of cirrus clouds, the characterization of ATAL requires cloud-filtering techniques to eliminate in-cloud measurements, and therefore a large dataset for a statistically-significant evaluation (e.g. 18 soundings are used in Vernier et al., 2015). We performed 17 COBALD soundings in NT16_{AUG}, but

Deleted: ozone values in DK17 compared to NT16_{AUG}, again suggesting stronger convective activity in the ASM 2017 than in 2016. Ozone depletion extending into the Confined LS confirms that the influence of deep convection on the composition of the UTLS persists up to altitudes well above the CPT, due to the horizontal confinement in ASMA. The fact that this feature vanishes in the Free LS (Panel c), suggests that

Deleted: is a good measure of the topmost extent of the anti-cyclonic confinement.

Deleted: These evidence show that, in the ASM system, the top height of the horizontal confinement in ASMA controls the distribution and variability of water vapor and ozone in the lowermost stratosphere, rather than CPT height as it is in the conventional understanding of the TTL.¶

Deleted: 3

Deleted: Panel

Deleted: .)

Deleted: Panel

Deleted: UT

Deleted: Panels

Deleted: , Panel a

Deleted: between

Deleted: , confirming that the ASM 2017 season was indeed extraordinary in terms of strong convection, and also suggesting particularly high

Deleted: ASMA 2017

Deleted: , Panels

Deleted: (e.g. see Figure 10, Panel f) and evaporate at higher levels in the Confined LS, similarly but likely more frequently than was found in the tropics (Corti et al., 2008). We consider this to be the reason for the isolated H₂O maximum above the CPT observed in DK17 (Figure 7, Panel b), which is, to our knowledge, unparalleled in the tropics. ¶

Deleted: Finally, here

Deleted: but as already mentioned,

Deleted: and validation of the Cloud-Aerosol Lidar and Infrared Pathfinder Satellite Observation (CALIPSO) satellite retrieval

Deleted: In this

Deleted: section

due to logistical constraints only 3 could be realized during the DK17 campaign, which furthermore mostly sampled cloudy conditions in the ATTL. For this reason, a clear-sky aerosol BSR profile cannot be established from the DK17 dataset. On the other hand, the 3 COBALD soundings available from NT16_{NOV} are almost fully clear-sky measurements and therefore allow to calculate a clear-sky aerosol BSR profile. The NT16_{NOV} measurements provide a useful reference state of background aerosols, without ASMA confinement and without supply of aerosols and precursor gases from the monsoonal deep convection, for comparison with NT16_{AUG}. In the following, we first provide an overview of the main characteristics of the observed cirrus clouds, and then detail the cloud-filtering technique and ATAL detection during the year 2016.

Deleted: , providing a useful reference state of background aerosols (i.e. without ASMA confinement) for comparison with NT16_{AUG}

6.1 Cirrus clouds

Figure 10 shows individual soundings as examples of thin cirrus clouds observed during the NT16_{AUG} (Panels a-d) and DK17 (e-f) campaigns. Along with the temperature and ice saturation profiles, we show BSR at 455 nm (BSR_{455}), BSR at 940 nm (BSR_{940}), and color index (CI). Color index is defined as the 940-to-455 nm ratio of the aerosol component of BSR, i.e. $CI = (BSR_{940} - 1)/(BSR_{455} - 1)$. CI has the property of being independent of number density, hence it is a useful indicator of particle size (e.g. Cirisian et al., 2014) as long as particles are sufficiently small, so that Mie scattering oscillations are avoided. Based on the size-dependence of CI, considerations on the typical size range of ice crystals and aerosol droplets, and the evaluation of ice saturation measurements by CFH, a threshold of $CI = 7$ was empirically developed to discriminate in-cloud ($CI > 7$) from clear-sky measurements ($CI < 7$) (Vernier et al., 2015). This helps discerning the BSR features in Figure 10 as either ice cloud or aerosol signal, and is also used as a threshold for cloud-filtering. For example, in sounding NT004 (Panel a), the sharp feature at 145 hPa with $CI \approx 10$ is likely an ice cloud (note the concomitant ice supersaturation above the thin cloud layer, suggesting sedimentation), while the broad enhancement in BSR between 95-140 hPa without CI enhancement is the signal of ATAL. The main common characteristics of the cirrus clouds in Figure 10 is their very small spatial and optical thickness, with $BSR_{940} < 20$, while much larger values ($BSR_{940} \gg 100$) are expected in homogeneously-nucleated cirrus clouds, as often observed in the midlatitudes (e.g. Brabec et al., 2012; Cirisian et al., 2014), and as also shown by the thick outflow cirrus below 120 hPa in DK002 (Panel f). Low BSR indicates low ice crystal number densities, suggesting that these clouds are most likely formed by heterogeneous nucleation on solid ice nuclei, rather than by homogeneous freezing of sulfate aerosol liquid droplets. This hypothesis is currently being investigated by a dedicated microphysical modeling study. Similarly thin cirrus clouds were observed in more than half of the COBALD soundings in NT16_{AUG} (9 out of 17), therefore they occur very frequently in the ASMA, and they were often found embedded within the ATAL. (Figure 10, panels a, e).

Deleted: in the ATTL

Deleted: Panels

Deleted: evidenced

Deleted: about

Deleted: , as shown in

Deleted: (P

Deleted: in

6.2 ATAL during the ASM 2016

Figure 11 shows all clear-sky (i.e. aerosol only) BSR_{455} data points and mean profiles from the NT16_{AUG} and NT16_{NOV} datasets. Similarly to Vernier et al. (2015), the cloud-filtering criterion that we applied consists of three thresholds from two independent

measurements, namely: $BSR_{940} < 2.5$ and $CI < 7$ from COBALD, and $S_{ice} < 0.7$ from CFH. Only data points which simultaneously fulfill all the three criteria above are classified as clear-sky and shown in Figure 11. The cloud-filtering method is illustrated by a scatter plot of BSR_{940} vs. CI shown in Figure S5 in supplementary material.

In NT16AUG, clear-sky BSR_{455} enhancement (i.e. mean value exceeding 1.04) starting approximately at the LRM (180 hPa) and extending up to the TOC (73 hPa) is the signature of ATAL (Figure 10), showing intensity and vertical extent comparable to those derived by satellite retrievals and previous COBALD measurements (Vernier et al., 2015; 2018). The aerosol enhancement covers both the ATTL and the CLS with maximum BSR_{455} at the CPT. The fact that ATAL's onset coincides with the LRM suggests that the mean convective outflow level is also the onset of horizontal confinement in ASMA. Maximum BSR_{455} at the CPT is possibly an effect of colder temperatures, driving the partitioning of more condensable material (e.g. nitrates, see Vernier et al., 2018) to the aerosol phase in ATAL. Above the CPT, the BSR_{455} enhancement gradually fades with altitude until the TOC, as the horizontal confinement effect of ASMA vanishes, which is consistent with the decreasing confined fraction of backward trajectories shown in Figure 5. Above the TOC, the ATAL signal merges with the Junge layer of stratospheric aerosols, which extends into the Free LS up to about 10 hPa. The clear-sky BSR_{455} enhancement is absent in NT16NOV at all altitudes in the UTLS (except for the Junge layer in the free stratosphere), showing that ATAL does not outlive the break-up of the anticyclonic vortex and the lack of supply of precursor gases by deep convection at the end of the ASM season.

7. Discussion and conclusions

We analyzed 63 balloon measurements of temperature, water vapor, ozone and aerosol backscatter, collected during the years 2016-2017 at the southern slopes of the Himalayas. The UTLS structure in this region exhibits a strong seasonal variability, with tropical features (sharp CPT) during the ASM, and midlatitudinal features (large LRT-CPT separation) during the post-monsoon season. To analyze the structure of the UTLS during the ASM season, we formulate a framework composed of three thermodynamically significant levels (LRM, CPT, TOC) and two layers (ATTL, CLS) illustrated in Figure 6. Figure 12 summarizes the mean profiles of temperature, $d\theta/dz$, H_2O mixing ratio, O_3 mixing ratio, ice saturation and aerosol BSR_{455} measured during NT16AUG (top panel) and DK17 (bottom panel), highlighting the relevance of these levels and layers.

During both the ASM season campaigns, the isentropic level of the LRM ($\theta = 362-364$ K) was higher than in previous measurements in the deep tropics ($\theta \approx 345$ K) (Gettelman and de F. Forster, 2002; Pan et al., 2014) and in the Tibetan plateau (355-360 K) (Bian et al., 2012), suggesting that convection is very deep-penetrating at the southern slopes of the Himalayas. The CPT ($\theta = 382-384$ K) was also higher than at tropical sites (375 K) (Gettelman and de F. Forster, 2002; Pan et al., 2014) but lower than above the Tibetan plateau (390 K) (Bian et al., 2012), which is consistent with the "bulging" of the CPT in ASMA (e.g. Pan et al., 2016) and suggests an orographic influence. The average LRM and CPT occur at higher altitude in DK17 compared to NT16AUG (400-600 m), but due to colder temperatures in DK17 (on average 5 K at the CPT), the shift in potential temperature space is small (1.5-2 K). We also note that in DK17 the TOC coincides with a local maximum in the thermal stability profile ($d\theta/dz$), which is the same feature as the level of maximum stability defined by Sunilkumar et al. (2017).

Deleted: S4

Deleted: CALIPSO

Deleted: soundings

Deleted: sian

Deleted: Confined

Deleted: , suggesting that the LRM (i.e. the mean convective outflow level) is also the onset of the horizontal confinement in ASMA, and the CPT the level of maximum strength of confinement

Deleted: by

Deleted: (see Figure 5)

Deleted: As expected, the aerosol enhancement is absent in NT16NOV

Deleted: have

Deleted: in the region of the southern slopes of the Himalayas

Deleted: NT16AUG campaign took place over one month (2-31 August) with average frequency of one balloon sounding per day, hence covering roughly one third of the ASM 2016...

Deleted: typically

Deleted: characteristics

Deleted: season due to deep convection, and "

Deleted: -

Deleted: e"

Deleted: separated

Deleted: and

Deleted: dry

Deleted: Therefore, for the analysis of our monsoon-season...

Deleted: Figure 13 summarizes mean profiles of the UTLS...

Deleted: tropical Western Pacific and Central America

Deleted: possibly

Deleted: ing

Deleted: It is also interesting to notice that, in both dataset...

Deleted: are found at lower pressures

Deleted: (by about 10 hPa),

Deleted: concomitant

Deleted: around

In both NT16_{AUG} and DK17, high H₂O and low O₃ were found in the ATTL and CLS, which is the signature of deep convection, extending up to 1.5-2 km above the CPT. Convective features are more pronounced in DK17 compared to NT16_{AUG}, suggesting that convective activity at the southern slopes of the Himalayas was more intense during the ASM season 2017 compared to 2016. In particular, an isolated H₂O maximum in the CLS was observed in DK17, which we argue it may be due to overshooting convection, as previously observed by Corti et al. (2008) and modelled by Dauhut et al. (2015; 2016).

The fact that the average CPTs in our datasets occur at lower potential temperatures than previously found above the Tibetan plateau suggests that, in addition to slow ascent and overshooting convection (discussed in Section 5.3), isentropic transport from the Tibetan plateau (below CPT) to the southern slopes of the Himalayas (above CPT) might also contribute to the high H₂O observed in the CLS. Nevertheless, since the isentropic level of the CPT is subject to strong instantaneous perturbations associated with convection and wave activity (e.g. Boehm and Verlinde, 2000; Sherwood et al., 2003; Munchak and Pan, 2014; Muhsin et al., 2018), a conclusion based on just the average CPT from a limited number of profiles is to be taken with caution, and further investigations will be required to assess the relevance of the different transport pathways.

The high H₂O observed in the CLS is particularly interesting because of its potential implications for stratospheric moistening. The air masses in the CLS have already crossed the CPT, hence will be unlikely subject to further dehydration, so it appears that the high H₂O in this layer is prone to be lifted further and mixed into the (drier) free stratosphere. However, it was shown that vertical transport above the ASMA might not be very efficient due to the slow ascending velocities of the Brewer-Dobson circulation in this region and season, and that the most efficient transport pathway is quasi-horizontal transport through the horizontal boundaries of ASMA and subsequent upwelling in the stratosphere above the deep tropics (Pan et al., 2016). Therefore, the fate of the air masses in the CLS (hence the moistening potential of the high H₂O in this layer) needs to be addressed by explicitly taking into account the horizontal motion of the air, which we do not investigate in this work.

Cloud-filtering of the aerosol backscatter reveals the signature of ATAL, extending from the LRM to the TOC with maximum backscatter at the CPT, and with similar BSR enhancement as in previous measurements from Lhasa, China (Vernier et al., 2015). No aerosol enhancement was found in NT16_{NOV}. In both NT16_{AUG} and DK17, ice saturation is minimum at the LRM and increases in the ATTL, similarly to as in the tropics (Vömel et al., 2002). Due to the much cold temperatures, average S_{ice} in DK17 is remarkably higher than in NT16_{AUG}, as well as than in previous measurements from the Tibetan plateau (Bian et al., 2012). Numerous thin cirrus clouds were detected during the NT16_{AUG} and DK17 campaigns (often embedded in ATAL), and their optical properties suggest they might be formed by heterogeneous freezing.

Our analysis provides a comprehensive and high-resolution overview of the UTLS structure and composition at the southern slopes of the Himalayas. The thermodynamically-significant levels and layers that we identify offer physically-meaningful boundaries for the interpretation of the observed vertical distributions of water vapor, ozone and aerosols in ASMA, and the extents of enhanced H₂O and aerosols (ATAL) above the CPT are in good agreement with the top of anticyclonic confinement estimated from air mass backward trajectories. Our approach based on significant levels, rather than fixed pressure or altitude stacks, also provides useful diagnostics for the comparison of our in-situ measurements with global climate model outputs.

Moved down [6]: Due to extremely cold temperatures, average S_{ice} in DK17 is remarkably higher than in NT16_{AUG}, as well as than in previous measurements from the Tibetan plateau (Bian et al., 2012).

Deleted: Ozone mixing ratio in DK17 shows a slight minimum above the LRM, which indicates strong convection (Vömel et al., 2002; Paulik and Birner, 2012) and was not observed in NT16_{AUG}. In both datasets, water vapor is higher in the Confined LS compared to the Free LS (see also Figure 8), and in DK17 the H₂O mean profile shows a local maximum about 1 km above the CPT. This feature contradicts the common conceptual understanding of TTL, which claims no water vapor variability above the CPT (Pan et al., 2014), and we suggest this is due to overshooting convection injecting condensed-phase ice directly above the CPT, which subsequently evaporate and hydrate the CLS. Ice saturation is minimum at the LRM and increases in the ATTL, similarly to as in the tropics (Vömel et al., 2002). Due to extremely cold temperatures, average S_{ice} in DK17 is remarkably higher than in NT16_{AUG}, as well as than in previous measurements from the Tibetan plateau (Bian et al., 2012). Aerosol Due to extremely cold temperatures, average S_{ice} in DK17 is remarkably higher than in NT16_{AUG}, as well as than in previous measurements from the Tibetan plateau (Bian et al., 2012).

Deleted: enhancement of the ATAL was detected in NT16_{AUG}

Deleted: vertical extent and

Deleted: intensity

Deleted: On average, ATAL extends from the LRM to the TOC with maximum backscatter at the CPT, suggesting that the mean convective outflow level (i.e. the LRM) is also the onset of the horizontal confinement in ASMA, CPT its level of maximum strength, and TOC its topmost extent.

Moved (insertion) [6]

Deleted: extremely

Deleted: In conclusion, o

Deleted: shows that the composition of the tropopause transition layer and the lowermost stratosphere within the ASM anticyclone are influenced by deep convection up to 1.5-2 km above the cold-point tropopause, due to the horizontal confinement effect of ASMA. Hence, the vertical distributions and variability of water vapor, ozone and aerosols in this region are controlled by the topmost extent of the anticyclonic confinement, rather than the altitude of the cold-point tropopause, as it is in the conventional understanding of the "generic" TTL. This is shown by enhanced water vapor and aerosol backscatter found in the confined lower stratosphere, in [...]

Deleted: thermodynamic

Deleted: physically-meaningful

As often mentioned throughout the paper, a wide range of modeling, interpretation and comparison studies are ongoing, aiming to explore the different insights offered by this dataset, and to assess its relevance in the context of stratospheric moistening via the ASMA system and related transport pathways. These investigations include microphysical model simulations, Lagrangian trajectory analyses, instrumental studies and comparisons with other in-situ measurements, such as the airborne Geophysica-M55 measurements during the StratoClim 2017 aircraft campaign and balloon soundings performed from various stations in the Tibetan plateau during the years 2013-2'17, as well as comparisons with different global modeling products. ▼

Deleted: inter

Deleted: , inter

Deleted: s (including

Deleted:)

Deleted: Further ongoing studies address the interactions of large-scale dynamics with the thermal structure of the UTLS and linkages to monsoon precipitation, evidence of overshooting convection and Lagrangian air mass origin analysis.

References

- Bergman, J. W., Fierli, F., Jensen, E. J., Honomichl, S., and Pan, L. L.: Boundary layer sources for the Asian anticyclone: Regional contributions to a vertical conduit, *J. Geophys. Res. Atmos.*, 118, 2560-2575, doi:10.1002/jgrd.50142, 2013
- Bian, J., Pan, L. L., Paulik, L., Vömel, H., Chen, H., and Lu, D.: In situ water vapor measurements in Lhasa and Kunming during the Asian summer monsoon, *Geophys. Res. Lett.*, 39, L19808, doi:10.1029/2012GL052996, 2012
- Boehm, M. T., and Verlinde, J.: Stratospheric influence on upper tropospheric tropical cirrus, *Geophys. Res. Lett.*, 27, 19, 3209-3212, 2000
- Brabec, M., Wienhold, F. G., Luo, B. P., Vömel, H., Immler, F., Steiner, P., Hausammann, E., Weers, U. and Peter, T.: Particle backscatter and relative humidity measured across cirrus clouds and comparison with microphysical cirrus modelling, *Atmos. Chem. Phys.*, 12, 9135-9148, doi:10.5194/acp-12-9135-2012, 2012
- Bucholtz, A.: Rayleigh-scattering calculations for the terrestrial atmosphere, *Appl. Optics*, 34, 15, 1995
- Cirisian, A., Luo, B. P., Engel, I., Wienhold, F. G., Sprenger, M., Krieger, U. K., Weers, U., Romanens, G., Levrat, G., Jeannot, P., Ruffieux, D., Philipona, R., Calpini, B., Spichtinger, P. and Peter, T.: Balloon-borne measurements of midlatitude cirrus clouds, *Atmos. Chem. Phys.*, 14, 7341-7365, doi:10.5194/acp-14-7341-2014, 2014
- Corti, T., Luo, B. P., de Reus, M., Brunner, D., Cairo, F., Mahoney, M. J., Martucci, G., Matthey, R., Mitev, V., dos Santos, F. H., Schiller, C., Shur, G., Sitnikov, N. M., Spelten, N., Vössing, H. J., Borrmann, S., and Peter, T.: Unprecedented evidence for deep convection hydrating the tropical stratosphere, *Geophys. Res. Lett.*, 35, L10810, doi:10.1029/2008GL033641, 2008
- Dauhut, T., Chaboureaud, J.-P., Escobar, J., and Mascart, P.: Large-eddy simulations of Hector the convective making the stratosphere wetter, *Atmos. Sci. Lett.*, 16, 135-140, DOI:10.1002/asl2.534, 2015
- Dauhut, T., Chaboureaud, J.-P., Escobar, J., and Mascart, P.: Giga-LES of Hector the Convective and Its Two Tallest Updrafts up to the Stratosphere, *J. Atmos. Sci.*, 73, 5041-5060, DOI:10.1175/JAS-D-16-0083.1, 2016
- Dethof, A., O'Neill, A., Slingo, J. M., and Smit, H. G. J.: A mechanism for moistening the lower stratosphere involving the Asian summer monsoon, *Q. J. R. Meteorol. Soc.*, 125, 1079-1106, 1999

Engel, I., Luo, B. P., Khaykin, S. M., Wienhold, F. G., Vömel, H., Kivi, R., Hoyle, C. R., Gross, J.-U., Pitts, M. C., and Peter, T.: Arctic stratospheric dehydration - Part 2: Microphysical modeling, *Atmos. Chem. Phys.*, 14, 3231-3246, doi:10.5194/acp-14-3231-2014, 2014

Fadnavis, S., Semeniuk, K., Pozzoli, L., Schultz, M. G., Ghude, S. D., Das, S., and Kakaktar, R.: Transport of aerosols into the UTLS and their impact on the Asian monsoon region as seen in a global model simulation, *Atmos. Chem. Phys.*, 13, 8771-8786, doi:10.5194/acp-13-8771-2013, 2013

Fadnavis, S., Schultz, M. G., Semeniuk, K., Mahajan, A. S., Pozzoli, L., Sonbawne, S., Ghude, S. D., Kiefer, M., and Eckert, E.: Trends in peroxyacetyl nitrate (PAN) in the upper troposphere and lower stratosphere over southern Asia during the summer monsoon season: regional impacts, *Atmos. Chem. Phys.*, 14, 12725-12743, doi.org/10.5194/acp-14-12725-2014, 2014

Fu, R., Hu, Y., Wright, J. S., Jiang, J. E., Dickinson, R. E., Chen, M., Filipiak, M., Read, W. G., Waters, J. W., and Wu, D. L.: Short circuit of water vapor and polluted air to the global stratosphere by convective transport over the Tibetan plateau, *Proc. Natl. Acad. Sci. USA*, 103, 15, 5664, doi:10.1073/pnas.0601584103, 2006

Fueglistaler, S., Dessler, A. E., Dunkerton, T. J., Folkins, I., Fu, Q., and Mote, P. W.: Tropical tropopause layer, *Rev. Geophys.*, 47, RG1004, doi:10.1029/2008RG000267, 2009

Garny, H. and Randel, W.: Dynamic variability of the Asian monsoon anticyclone observed in potential vorticity and correlations with tracer distributions, *J. Geophys. Res. Atmos.*, 118, 13421-13433, doi:10.1002/2013JD020908, 2013

Garny, H. and Randel, W.: Transport pathways from the Asian monsoon anticyclone to the stratosphere, *Atmos. Chem. Phys.*, 16, 2703-2718, doi:10.5194/acp-16-2703-2016, 2016

Gettelman, A. and de F. Forster, P. M.: A climatology of the Tropical Tropopause Layer, *J. Meteorol. Soc. Japan*, 80, 911-924, 2002

[Gottschaldt, K.-D., Schlager, H., Baumann, R., Sinh Cai, D., Eyring, V., Graf, P., Grewe, V., Jöckel, P., Jurkat-Witschas, T., Voigt, C., Zahn, A., and Ziereis, H.: Dynamics and composition of the Asian summer monsoon anticyclone, *Atmos. Chem. Phys.*, 18, 5655-5675, <http://doi.org/10.5194/acp-18-5655-2018>, 2018](#)

Heath, N. K. and Fuelberg, H. E.: Using a WRF simulation to examine regions where convection impacts the Asian monsoon anticyclone, *Atmos. Chem. Phys.*, 14, 2055-2070, doi:10.5194/acp-14-2055-2014, 2014

[Hoskins, B. J., and Rodwell, M. J.: A Model of the Asian Summer Monsoon. Part I: The Global Scale, *J. Atmos. Sci.*, 52, 1329-1340, 1995](#)

InterMet: iMet-1-RS 403 MHz Research Radiosonde, Data Sheet, International Met Systems, 3854 Broadmoore SE, Grand Rapids, MI, USA, http://www.intermetsystems.com/ee/pdf/iMet-1_RS_Data_130530.pdf, 2006 (accessed 4 January 2018)

Jordan, A. and Hall, E.: SkySonde User Manual, Version 1.9, <ftp://aftp.cmdl.noaa.gov/user/jordan/SkySonde%20User%20Manual.pdf>, 2016 (accessed 4 January 2018)

Komhyr, W. D.: Electrochemical Concentration Cells for gas analysis, *Ann. Geophys.*, 25, 203-210, 1969

Deleted: Highwood, E. J. and Hoskins, B. J.: The tropical tropopause, *Q. J. R. Meteorol. Soc.*, 125, 1579-1604, 1998
Holton, J. R. and Gettelman, A.: Horizontal transport and the dehydration of the stratosphere, *Geophys. Res. Lett.*, 28, 14, 2799-2802, 2001

Kräuchi, A., Philipona, R., Romanens, G., Hurst, D. F., Hall, E. G., and Jordan, A. F.: Controlled weather balloon ascents and descents for atmospheric research and climate monitoring, *Atmos. Meas. Tech.*, 9, 929-938, doi:10.5194/amt-9-929-2016, 2016

Krishnamurti, T. N. and Bhalme, H. N.: Oscillations of a Monsoon System. Part I. Observational Aspects, *J. Atmospheric Sci.*, 33, 1937-1954, 1976

Krotkov, N. A., McLinden, C. A., Li, C., Lamsal, L. N., Celarier, E. A., Marchenko, S. V., Swartz, W. H., Bucsela, E. J., Joiner, J., Buncan, B. N., Boersma, F. K., Veeckind, P. J., Levelt, P. F., Fioletov, V. E., Dickerson, R. R., He, H., Lu, Z., and Streets, D. G.: Aura OMI observations of regional SO₂ and NO₂ pollution changes from 2005 to 2015 et al. (2016), *Atmos. Chem. Phys.*, 16, 4605-4629, doi:10.5194/acp-16-4605-2016, 2016

Kumar, R., Naja, M., Venkataramani, S., and Wild, O.: Variations in surface ozone at Nainital: A high-altitude site in the central Himalays, *J. Geophys. Res.*, 115, D16302, doi:10.1029/2009JD013715, 2010

[Kunz, A., Konopka, P., Müller, R., and Pan, L. L.: Dynamical tropopause based on isentropic potential vorticity gradients, *J. Geophys. Res.*, 116, D01110, doi:10.1029/2010JD014343, 2011](#)

[Lawrence, M. G., and Lelieveld, J.: Atmospheric pollutant outflow from southern Asia: a review, *Atmos. Chem. Phys.*, 10, 11017-11096, doi:10.5194/acp-10-11017-2010, 2010](#)

[Muhsin, M., Sunilkumar, S. V., Venkat Ratnam, M., Parameswaran, K., Krishna Murthy, B., and Emmanuel, M.: Effect of convection on the thermal structure of the troposphere and lower stratosphere including the tropical tropopause layer in the South Asian monsoon region, *J. Atmospheric Sol.-Terr. Phys.*, 169, 52-65, <https://doi.org/10.1016/j.jastp.2018.10.016>, 2018](#)

[Munchak, L. A., and Pan, L. L.: Separation of the lapse rate and the cold point tropopauses in the tropics and the resulting impact on cloud top-tropopause relationships, *J. Geophys. Res. Atmos.*, 119, 7963-7978, doi:10.1002/2013JD021189, 2014](#)

[Murphy, D. M. and Koop, T.: Review of the vapour pressures of ice and supercooled water for atmospheric applications, *Q. J. R. Meteorol. Soc.*, 131, 1539-1565, doi:10.1256/qj.04.94, 2005](#)

Nützel, M., Dameris, M., and Garny, H.: Movements, drivers and bimodality of the South Asian High, *Atmos. Chem. Phys.*, 16, 14755-14774, doi:10.5194/acp-16-14755-2016, 2016

Oelsner, P. and Tietz, R.: GRUAN Monitor MW41 and the Vaisala RS41 Additional Sensor Interface, Technical Note 8 (GRUAN-TN-8), https://www.gruan.org/gruan/editor/documents/gruan/GRUAN-TN-8_GRUAN-Monitor-MW41-and-Vaisala_RS41_Additional_Sensor_Interface_v1.0.pdf, 2017 (accessed 4 January 2018)

[Orbe, C., Waugh, D. W., and Newman, P. A.: Air-mass origin in the tropical lower stratosphere: The influence of Asian boundary layer air, *Geophys. Res. Lett.*, 42, 4240-4248, <https://doi.org/10.1002/2015GL063937>, 2015](#)

Pan, L. L., Paulik, L. C., Honomichl, S. B., Munchak, L. A., Bian, J., Selkirk, H. B., and Vömel, H.: Identification of the tropical tropopause transition layer using the ozone - water vapor relationship, *J. Geophys. Res. Atmos.*, 119, 3586-3599, doi:10.1002/2013JD020558, 2014

Deleted: Mote, P. W., Rosenlof, K. H., McIntyre, M. E., Carr, S. E., Gille, J. C., Holton, J. R., Kinnerson, J. S., Pumphrey, H. C., Russell III, J. M., and Waters, J. W.: An atmospheric tapo recorder: The imprint of tropical tropopause temperatures on stratospheric water vapor, *J. Geophys. Res.*, 101, D2, 3989-4006, 1996

- Pan, L. L., Honomichl, S. B., Kinnison, D. E., Abalos, M., Randel, W. J., Bergman, J. W., and Bian, J.: Transport of chemical tracers from the boundary layer to stratosphere associated with the dynamics of the Asian summer monsoon, *J. Geophys. Res. Atmos.*, 121, 14159-14174, doi:10.1002/2016JD025616, 2016
- Park, M., Randel, W. J., Kinnison, D. E., Garcia, R. R., and Choi, W.: Seasonal variation of methane, water vapor, and nitrogen oxides near the tropopause: Satellite observations and model simulations, *J. Geophys. Res.*, 109, D03302, doi:10.1029/2003JD003706, 2004
- Park, M., Randel, W. J., Gettelman, A., Massie, S. T., and Jiang, J. H.: Transport above the Asian summer monsoon anticyclone inferred from Aura Microwave Limb Sounder tracers, *J. Geophys. Res.*, 112, D16309, doi:10.1029/2006JD008294, 2007
- Park, M., Randel, W. J., Emmons, L. K., Bernath, P. F., Walker, K. A., and Boone, C. D.: Chemical isolation in the Asian monsoon anticyclone observed in Atmospheric Chemistry Experiment (ACE-FTS) data, *Atmos. Chem. Phys.*, 8, 757-764, www.atmos-chem-phys.net/8/757/2008/, 2008
- Paulik, L. C. and Birner, T.: Quantifying the deep convective temperature signal within the tropical tropopause layer (TTL), *Atmos. Chem. Phys.*, 12, 12183-12195, doi:10.5194/acp-12-12183-2012, 2012
- Ploeger, F., Gottschling, C., Griessbach, S., Gross, J.-U., Guenther, G., Konopka, P., Müller, R., Riese, M., Stroh, F., Tao, M., Ungermann, J., Vogel, B., and von Hobe, M.: A potential vorticity-based determination of the transport barrier in the Asian summer monsoon anticyclone, *Atmos. Chem. Phys.*, 15, 13145-13159, doi:10.5194/acp-15-13145-2015, 2015
- Randel, W. J. and Park, M.: Deep convective influence on the Asian summer monsoon anticyclone and associated tracer variability observed with Atmospheric Infrared Sounder (AIRS), *J. Geophys. Res.*, 111, D12314, doi:10.1029/2005JD006490, 2006
- Randel, W. J., Wu, F., Gettelman, A., Russel III, J. M., Zawodny, J. M., and Oltmans, S. J.: Seasonal variation of water vapor in the lower stratosphere observed in Halogen Occultation Experiment data, *Geophys. Res.*, 106, 14313-14325, JD900048509.00, 2001
- Randel, W., Udelhofen, P., Fleming, E., Geller, M., Gelman, M., Hamilton, K., Karoly, D., Ortland, D., Pawson, S., Swinbank, R. Wu, F., Baldwin, M., Chanin, M. L., Keckhut, P., Labitzke, K., Remsberg, E., Simmons, E., and Wu, D.: The SPARC Intercomparison of Middle-Atmosphere Climatologies, *J. Clim.*, 17, 986-1003, 2003
- Randel, W. J., Park, M., Emmons, L., Kinnison, D., Bernath, P., Walker, K. A., Boone, C., and Pumphrey, H.: Asian Monsoon Transport of Pollution to the Stratosphere, *Science*, 328, 611-613, doi:10.1126/science.1182274, 2010
- [Randel, W. J., and Jensen, E. J.: Physical processes in the tropical tropopause layer and their roles in a changing climate, *Nat. Geosci.*, 6, 169-176, DOI:10.1038/NGEO1733, 2013](#)
- [Rauthe-Schöch, A., Baker, A. K., Schuck, T. J., Brenninkmeijer, C. A. M., Zahn, A., Hermann, M., Stramann, G., Ziereis, H., van Velthoven, P. F. J., and Lelieveld, J.: Trapping, chemistry and export of trace gases in the South Asian summer monsoon observed during CARIBIC flights in 2008, *Atmos. Chem. Phys.*, 16, 3609-3629, doi:10.5194/acp-16-3609-2016, 2016](#)

Rosen, J. M. and Kjome, N. T.: Backscattersonde: a new instrument for atmospheric aerosol research, *Applied Optics*, 30, 12, 1552-1561, 1991

[Sherwood, S. C., Horinouchi, T., and Zeleznik, H. A.: Convective Impact on Temperatures Observed near the Tropical Tropopause, *J. Atmos. Sci.*, 60, 1847-1855, 2003](#)

5 Smit, H. G. J., Straeter, W., Johnson, B. J., Oltmans, S. J., Davies, J., Tarasick, D. W., Hoegger, B., Stubi, R., Schmidlin, F. J., Northam, T., Thompson, A. M., Witte, J. C., Boyd, I., and Posny, F.: Assessment of the performance of ECC-ozonesondes under quasi-flight conditions in the environmental simulation chamber: Insights from the Juelich Ozone Sonde Intercomparison Experiment (JOSIE), *J. Geophys. Res.*, 112, D19306, doi:10.1029/2006JD007308, 2007

10 [Sunilkumar, S. V., Muhsin, M., Venkat Ratnam, M., Parameswaran, K., Krishna Murthy, B. V., and Emmanuel, M.: Boundaries of tropical tropopause layer \(TTL\): A new perspective based on thermal and stability profiles, *J. Geophys. Res. Atmos.*, 122, 741-754, doi:10.1002/2016JD025217, 2017](#)

Thomason, L. W. and Vernier, J.-P.: Improved SAGE II cloud/aerosol categorization and observations of the Asian tropopause aerosol layer: 1989-2005, *Atmos. Chem. Phys.*, 13, 4605-4616, doi:10.5194/acp-13-4605-2013, 2013

15 [Ungermann, J., Ern, M., Kaufmann, M., Müller, R., Spang, R., Ploeger, F., Vogel, B., and Riese, M.: Observations of PAN and its confinement in the Asian summer monsoon anticyclone in high spatial resolution, *Atmos. Chem. Phys.*, 16, 8389-8403, doi:10.5194/acp-16-8389-2016, 2016](#)

Vaisala: Vaisala DigiCORA Sounding System MW41, Technical Reference, Vaisala Oyi, P.O. Box 26, FI 00421, Helsinki, Finland, <http://meteorology.lyndonstate.edu/~ATM/wp-content/uploads/2015/05/M211415EN-F.pdf>, 2014 (accessed 4 January 2018)

20 Vaisala: Vaisala Radiosonde RS41 Measurement Performance, White Paper, Vaisala, P.O. Box 26, FI 00421, Helsinki, Finland, <https://www.vaisala.com/sites/default/files/documents/WEA-MET-RS41-Performance-White-paper-B211356EN-B-LOW-v3.pdf>, 2017 (accessed 4 January 2018)

Vellore, R. K., Kaplan, M. L., Krishnan, R., Lewis, J. M., Sabade, S., Deshpande, N., Singh, B. B., Madhura, D. K., and Rama Rao, S. V. S.: Monsoon-extratropical circulation interactions in Himalayan extreme rainfall, *Clim. Dyn.*, 46, 3517-3546, doi:10.1007/s00382-015-2784-x, 2016

25 Vernier, J.-P., Thomason, L. W., and Kar, J.: CALIPSO detection of an Asian tropopause aerosol layer, *Geophys. Res. Lett.*, 38, L07804, doi:10.1029/2010GL046614, 2011

Vernier, J.-P., Fairlie, T. D., Natarajan, M., Wienhold, F. G., Bian, J., Martinsson, B. G., Crumeyrolle, S., Thomason, L. W., and Bedka, K. M.: Increase in upper tropospheric and lower stratospheric aerosol levels and its potential connection with Asian pollution, *J. Geophys. Res. Atmos.*, 120, 1608-1619, doi:10.1002/2014JD022372, 2015

30 [Vernier, J.-P., Fairlie, T. D., Deshler, T., Venkat Ratnam, M., Gadhavi, H., Kumar, B. S., Natarajan, M., Pandit, A. K., Akhil Raj, S. T., Hemanth Kumar, A., Jayaraman, A., Singh, A. K., Rastogi, N., Sinha, P. R., Kumar, S., Tiwari, S., Wegner, T., Baker, N., Vignelles, D., Stenchikov, G., Shevchenko, I., Smith, J., Bedka, K., Kesarkar, A., Singh, V., Bhate, J., Ravikiran,](#)

[V., Durga Rao, M., Ravindrababu, S., Patel, A., Vernier, H., Wienhold, F. G., Liu, H., Knepp, T. N., Thomason, L., Crawford, J., Ziemba, L., Moore, J., Crumeyrolle, S., Williamson, M., Berthet, G., Jégou, F., and Renard, J.-B.: BATAL The Balloon Measurement Campaigns of the Asian Tropopause Aerosol Layer, *Bull. Am. Meteorol. Soc.*, May 2018, 955-973, <https://doi.org/10.1175/BAMS-D-17-0014.1>, 2018](https://doi.org/10.1175/BAMS-D-17-0014.1)

5 Vogel, B., Günther, G., Müller, R., Gross, J.-U., Hoor, P., Krämer, M., Müller, S., Zahn, A., and Riese, M.: Fast transport from Southeast Asia boundary layer sources to Northern Europe: rapid uplift in typhoons and eastward eddy shedding of the Asian monsoon anticyclone, *Atmos. Chem. Phys.*, 14, 12745-12762, <https://doi.org/10.5194/acp-14-12745-2014>, 2014

Vogel, B., Günther, G., Müller, R., Gross, J.-U., and Riese, M.: Impact of different Asian source regions on the composition of the Asian monsoon anticyclone and of the extratropical lowermost stratosphere, *Atmospheric Chemistry and Physics*, 15, 13699-13716, doi:10.5194/acp-15-13699-2015, 2015

10 Vömel, H., Oltmans, S. J., Johnson, B. J., Hasebe, F., Shiotani, M., Fujiwara, M., Nishi, N., Agama, M., Cornejo, J., Paredes, F. and Enriquez, H.: Balloon-borne observations of water vapor and ozone in the tropical upper troposphere and lower stratosphere, *J. Geophys. Res.*, 107, D14, 4210, doi: 10.1029/2001JD000707, 2002

Vömel, H., David, D. E., and Smith, K.: Accuracy of tropospheric and stratospheric water vapor measurements by the cryogenic frost point hygrometer: Instrumental details and observations, *J. Geophys. Res.*, 112, D08305, doi:10.1029/2006JD007224, 2007

15 Vömel, H., Naebert, T., Dirksen, R., and Sommer, M.: An update on the uncertainties of water vapor measurements using Cryogenic Frostpoint Hygrometers, *Atmos. Meas. Tech.*, 9, 3755-3768, <https://doi.org/10.5194/amt-9-3755-2016>, 2016

Wendell, J. and Jordan, A.: iMet-1-RSB Radiosonde XDATA Protocol & Daisy Chaining, version 1.3, <ftp://aftp.cmdl.noaa.gov/user/jordan/iMet-1-RSB%20Radiosonde%20XDATA%20Daisy%20Chaining.pdf>, 2016 (accessed 4 January 2018)

20 Wernli, H. and Davies, H. C.: A Lagrangian-based analysis of extratropical cyclones. I: The method and some applications, *Q. J. R. Meteorol. Soc.*, 123, 467-489, 1997

World Meteorological Organization (WMO): Meteorology – A three-dimensional science: Second session of the commission for aerology, *World Meteorol. Organ. Bull.*, 4, 134-138, 1957

25 Yan, R. C., Bian, J., and Fan, Q. J.: The Impact of the South Asia High Bimodality on the Chemical Composition of the Upper Troposphere and Lower Stratosphere, *Atmos. Ocean. Sci. Lett.*, 4, 229-234, 2011

Acknowledgements

The research leading to these results has received funding from the European Community's Seventh Framework Programme (FP7/2007 - 2013) under grant agreement n° 603557 and the Swiss National Science Foundation in project n° 200021-117987. The use of ECMWF operational and ERA-Interim data is gratefully acknowledged. Support from the Director ARIES and the

ISRO ATCTM project is highly acknowledged for the observations at Nainital. [Support from the HiCCDRC group of Kathmandu University is highly acknowledged for the observations at Dhulikhel. Maxi Boettcher acknowledges funding from the Swiss National Science Foundation via grant 200020-165941.](#) The author Simone Brunamonti thanks Dr. Federico Fierli and Dr. Laura Pan for inspiring discussion.

5

10

15

20

25

30

Acronym	Description
Thermodynamic structure and features	
ASM	Asian summer monsoon
ASMA	Asian summer monsoon anticyclone
ATAL	Asian tropopause aerosol layer
ATTL	Asian tropopause transition layer
CLS	Confined lower stratosphere
CPT	Cold-point tropopause
LRM	Lapse-rate minimum
LRT	Lapse-rate tropopause
TOC	Top of confinement
UTLS	Upper troposphere - lower stratosphere
Measurement sites	
NT	Nainital, India (29.35°N, 79.46°E)
DK	Dhulikhel, Nepal (27.62°N, 85.54°E)
NT16 _{AUG}	Balloon campaign in NT in August 2016
NT16 _{NOV}	Balloon campaign in NT in November 2016
DK17	Balloon campaign in DK in July-August 2017

Table 1. List of the main acronyms used in this paper.

Commented [BS4]: New Table 1 added

Campaign	Time period	RS41	ECC	CFH	COBALD	Early burst
NT16 _{AUG}	2-31 Aug 2016	30* (0)	24 (2)	27 (1, 5)	17 (0)	4
NT16 _{NOV}	2-8 Nov 2016	5 (0)	5 (0)	5 (0, 1)	3 (1)	0
DK17	30 Jul-12 Aug 2017	28 (0)	12 (2)	11 (0, 4)	3 (0)	5
Total		63* (0)	41 (4)	43 (1, 10)	23 (1)	9

Table 2. Number of **balloon** soundings performed for each instrument and campaign period. In parentheses: number of soundings with instrumental malfunctionings (CFH: number of failures and contamination events, respectively). Early burst is defined as burst altitude < 25 km. (*) Note that iMet radiosondes were used for the first two soundings in NT16_{AUG} instead of RS41 (see Section 2).

Commented [BS5]: Former Table 1 renamed Table 2

Deleted: 1

Deleted: , station

Deleted: for

Deleted: -1-RSB

Deleted: -SGP

	NT16 _{AUG}				NT16 _{NOV}				DK17			
	<i>z</i> (km)	<i>p</i> (hPa)	<i>θ</i> (K)	<i>T</i> (°C)	<i>z</i> (km)	<i>p</i> (hPa)	<i>θ</i> (K)	<i>T</i> (°C)	<i>z</i> (km)	<i>p</i> (hPa)	<i>θ</i> (K)	<i>T</i> (°C)
LRM	13.3	180	360	-52.7	10.5	260	337.5	-43.6	13.7	169.5	362.5	-55
LRT	17.0	97.5	382	-76.8	16.0	108	378	-73.2	17.6	88	383.5	-81.7
CPT	17.0	97.5	382	-76.8	18.5	69.5	424	-75.3	17.6	88	383.5	-81.7
TOC	18.6	73	421.5	-73.7	<i>N.A.</i>	<i>N.A.</i>	<i>N.A.</i>	<i>N.A.</i>	19.5	63.5	441	-72.7

Table 3. Mean values of altitude (*z*), pressure (*p*), potential temperature (*θ*) and temperature (*T*) of the lapse rate minimum (LRM), lapse rate tropopause (LRT), cold-point tropopause (CPT) and top of confinement (TOC) levels during the three campaign periods, NT16_{AUG}, NT16_{NOV} and DK17. Note that for NT16_{NOV}, the definition of TOC is not applicable (N.A.).

Commented [BS6]: Former Table 2 renamed Table 3

Deleted: 2

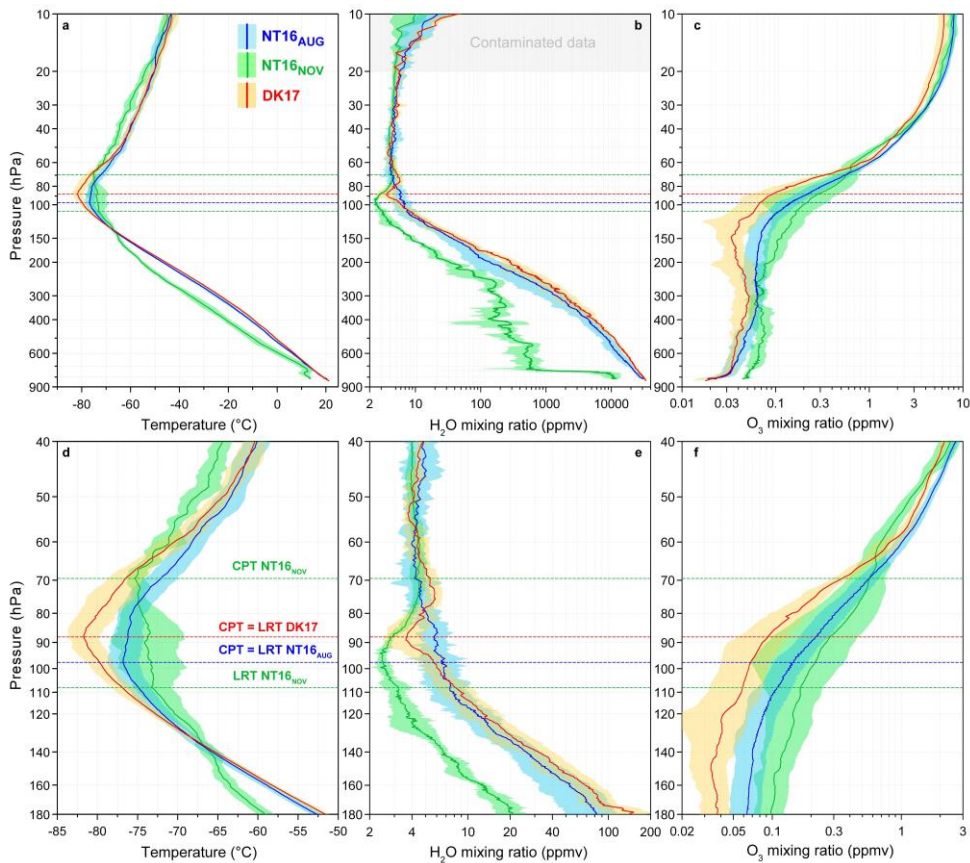


Figure 1. Mean profiles (solid lines) and standard deviations (color shading) of all measurements of temperature from RS41 (Panels a, d), H₂O mixing ratio from CFH (b, e), and O₃ mixing ratio from ECC (c, f) as a function of pressure, for NT16_{AUG} (blue), NT16_{NOV} (green) and DK17 (red). Dashed lines indicate the pressure levels of the average cold-point tropopause (CPT) and the lapse-rate tropopause (LRT) for the different datasets. Upper row (a-c): measured profiles from the surface to 10 hPa. Bottom row (d-f): zoom into the UTLS region (40-180 hPa). The grey shaded area in panel b indicates the region of contaminated CFH data (see Section 3).

Deleted: Horizontal

Deleted: , dashed

Deleted: , and the lapse-rate tropopause (LRT, dotted) for NT16_{NOV}

Deleted: tropopause

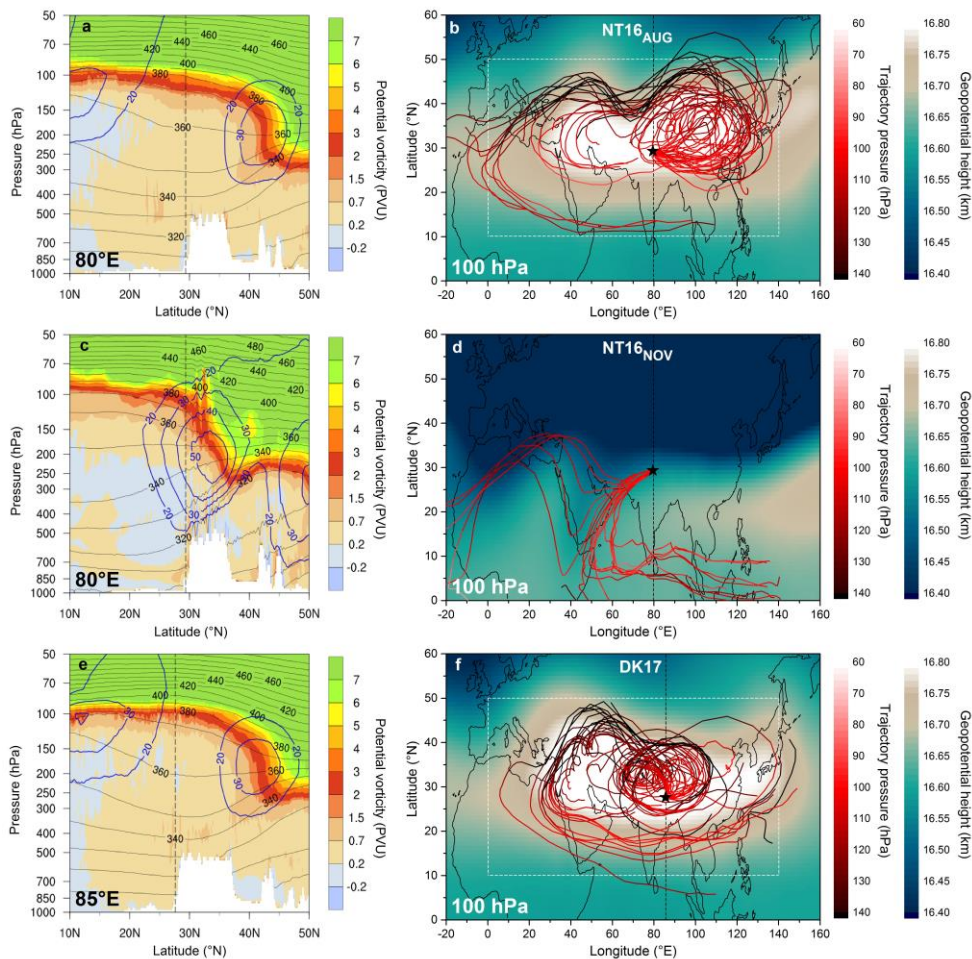


Figure 2. Left column: latitude-pressure cross-sections of: potential vorticity (color scale), potential temperature (black contours, in K), and total wind speed (blue contours, m/s) from ECMWF operational analysis data (horizontal resolution: 0.125° , vertical resolution: L137) averaged over the time periods of the NT16AUG (panel a, longitude 80°E), NT16NOV (panel c, longitude 80°E) and DK17 (panel e, longitude 85°E) campaigns, as given in Table 2. Black dashed lines show the latitude of NT (a, c) and DK (e). Right column:

Deleted: along longitude 80°E (Panels a,c) and 85°E (e),

Deleted: zonal

Deleted: and ice water content (white contours, 8 steps, log-scale between 0.1-1000 ppmm)

Deleted: for: 8 August 2016 at 00 UTC (a), 11 November 2016 00 UTC (c), and 5 August 2017, 12 UTC (e)

geopotential height at 100 from ECMWF analysis data averaged over the time periods of the NT16_{AUG} (b), NT16_{NOV} (d) and DK17 (f) campaigns (color scale), and 2-weeks LAGRANTO backward trajectories along ERA-Interim wind fields (horizontal resolution 1°, vertical resolution L60), initialized at 100 hPa at the time of each balloon sounding in NT16_{AUG} (Panel b), NT16_{NOV} (c), and DK17 (f), color-coded with pressure. Black dashed lines show the longitude of NT (a, c) and DK (e). The white dashed rectangle in panels (d, f) shows the approximated ASMA area used for the confined fraction calculation (10-50°N, 0-140°E; see Section 5.2). Note that, for NT16_{NOV}, trajectories started 6 h before and 6 h after each sounding are also included.

Deleted: (1°, L60)

Deleted: . Note that in Panel c (NT16_{NOV}),

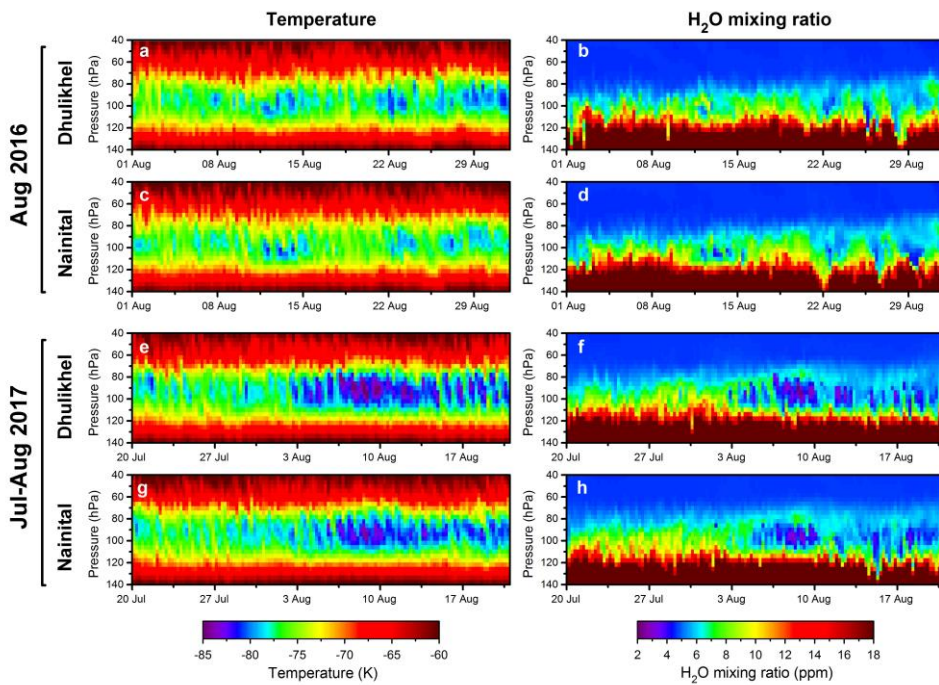


Figure 3. Time series of temperature (left column) and water vapor mixing ratio (right column) as a function of pressure, from ECMWF operational analysis data (6-hourly, horizontal resolution: 0.125° , vertical resolution: L137) for the locations of NT (Panels c, d, g, h) and DK (a, b, e, f) during 1-31 August 2016 (a-d) and 20 July-21 August 2017 (e-h).

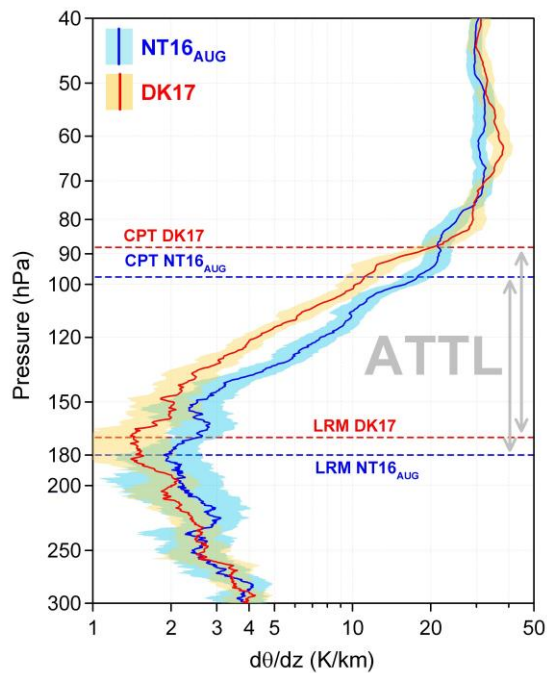


Figure 4. Figure 4. Mean profiles (solid lines) and standard deviations (color shading) of $d\theta/dz$ as a function of pressure, for NT16_{AUG} (blue) and DK17 (red). Horizontal dashed lines show the mean LRM and CPT for NT16 (blue) and DK17 (red). The ATTL regions for the two datasets are highlighted by grey arrows. Note that the mean profiles and standard deviations of $d\theta/dz$ were smoothed with a ± 5 hPa (about 250 m) moving average to reduce the noise contributions from the geometric altitude measurement by RS41.

Commented [BS7]: Former Figure 4 eliminated and replaced with former Figure 6 (modified)

Deleted: Comparison of temperature (Panels a, d), water vapor mixing ratio (b, e) and $d\theta/dz$ (c, f) mean profiles (solid lines) and standard deviations (color shading) of the NT16_{AUG} (blue) and DK17 (red) campaigns, with ECMWF operational data (mean profiles and standard deviation bars, purple) for the periods: 1-31 August 2016 (a-c), 29 July-13 August 2017 (d, f) and 3-13 August 2017 (e). Dashed lines show the mean CPT (Panels a, d) and LRM (c, f) in the different datasets. ECMWF operational data consists of analysis and forecast (horizontal resolution: 0.125° , vertical resolution: L137) combined by taking analysis data files (6-hourly) for every time step at 00, 06, 12 and 18 UTC, and forecast data files (1-hourly) at all other time steps, from the most recent available forecast run (i.e. for every day, forecast data files initialized at 00 UTC are used for 01-11 UTC, and forecast initialized at 12 UTC for 13-23 UTC). Note that different periods are selected for Panels d, f and e because, while the DK17 campaign started on 29 July 2017, CFH water vapor measurements only started on 3 August 2017 (see Table S1 in supplementary material).

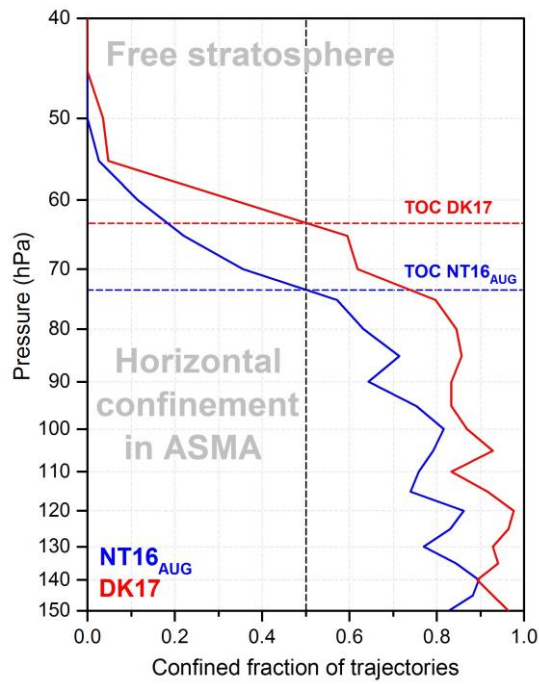


Figure 5. Confined fraction of trajectories (see Section 5.2) as a function of pressure for the NT16_{AUG} (blue) and DK17 (red) campaign periods. Dashed lines mark the TOC level for NT16 (blue) and DK17 (red) and the 50% confined fraction threshold (black).

Deleted: as a function of pressure (defined by 2-weeks backward trajectories, as described in Section 4.3)

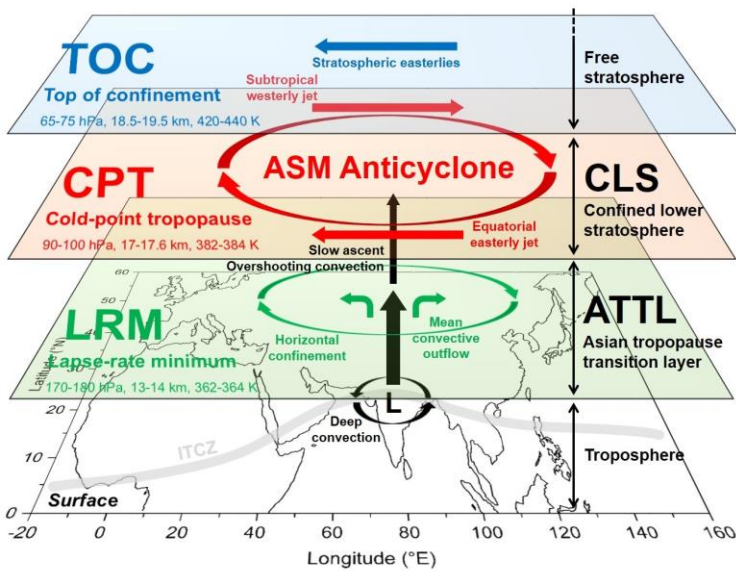


Figure 6. Schematics of the vertical structure of the UTLS above the southern slopes of the Himalayas. The Asian summer monsoon anticyclone (ASMA) consists of two layers, the Asian tropopause transition layer (ATTL) and the confined lower stratosphere (CLS). These layers are confined by three levels: the lapse rate minimum (LRM, green surface), the cold-point tropopause (CPT, red) and the top of confinement (TOC, blue). Dynamical features and relevant transport processes discussed in the paper are also sketched. Approximated pressure, altitude and potential temperature levels of the TOC, CPT and LRM derived from our NT16_{AUG} and DK17 measurements are displayed on the respective surfaces.

Commented [BS8]: Former Figure 6 moved to Figure 4 and replaced with former Figure 12.

Moved (insertion) [7]

Deleted: and main observed features

Deleted: Mean profiles (solid lines) and standard deviations (color shading) of temperature (Panel a), potential temperature (b) and $d\theta/dz$ (c), as a function of pressure, for NT16_{AUG} (blue) and DK17 (red). Horizontal lines show the mean CPT (dashed) and LRM (dotted) for NT16 (blue), and DK17 (red). The region of the Asian tropopause transition layer (ATTL) defined in Section 5.1 is also highlighted. Note that mean profiles and standard deviations of $d\theta/dz$ were smoothed with a ± 5 hPa (about 250 m) moving average to reduce the noise in the GPS geometric altitude measurement by RS41.

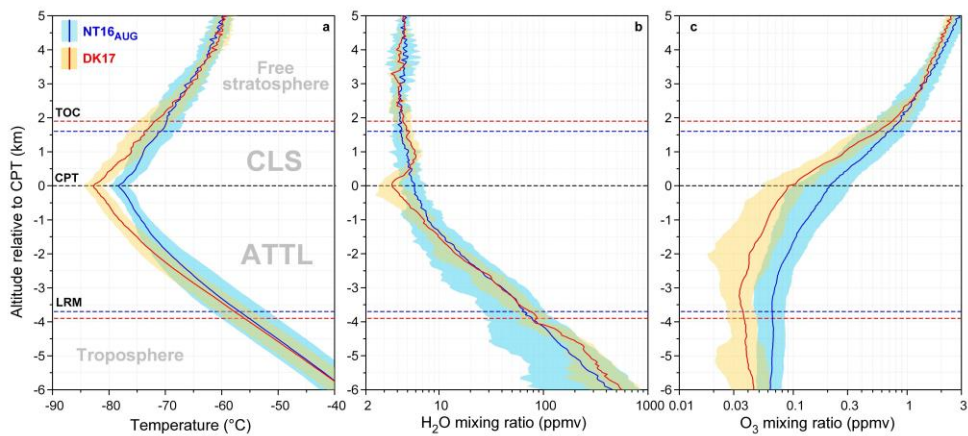


Figure 7. Mean profiles (solid lines) and standard deviations (color shading) of temperature (Panel a), H₂O mixing ratio (b) and O₃ mixing ratio (c) as a function of altitude relative to CPT, for NT16_{AUG} (blue) and DK17 (red). Dashed lines show the CPT (black) and the average LRM and TOC levels for NT16 (blue) and DK17 (red) (see labels in panel a). The four layers defined in Section 5.1 (troposphere, ATTL, CLS, and free stratosphere) are identified by grey labels.

Deleted: LRM levels for NT16 (blue), and DK17 (red). Dotted lines show the TOC levels for NT16 (blue), and DK17 (red)

Deleted: UT

Deleted: , FLS

Deleted: also highlighted

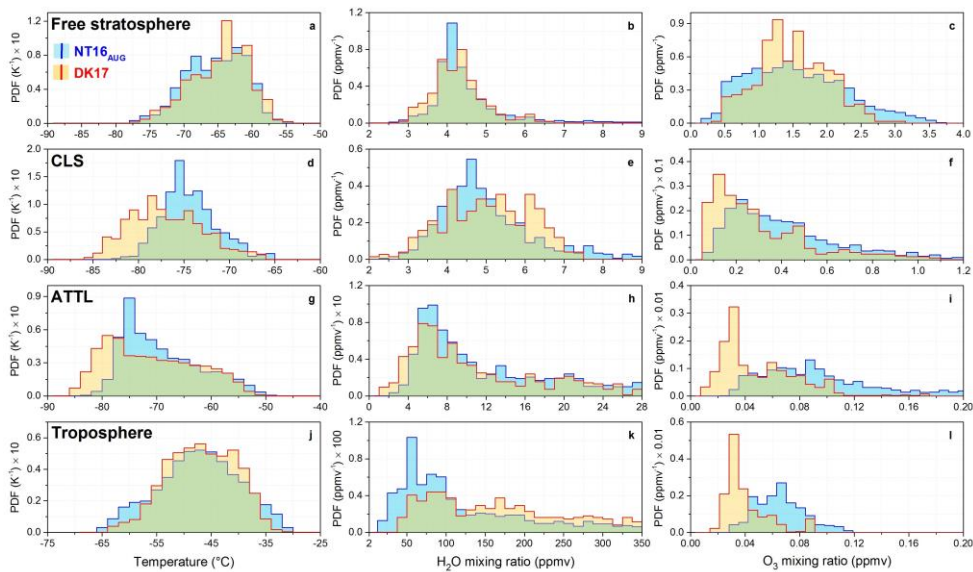


Figure 8. Probability density functions (PDFs) of temperature (left column), H₂O mixing ratio (center column) and O₃ mixing ratio (right column), calculated in the altitude regions of the free stratosphere (panels a-c), CLS (d-f), ATTL (g-h) and troposphere (j-l) as defined in Section 5.1, for NT16_{AUG} (blue) and DK17 (red).

Deleted: Free LS

Deleted: FLS, P

Deleted: Confined

Deleted: CLS,

Deleted: sian

Deleted: ATTL,

Deleted: upper

Deleted: UT, Panels

Deleted: -

Deleted: PDFs of the UT region are calculated for altitudes between LRM and CPT - 6 km, while for the FLS between CPT and CPT + 5 km (i.e. the altitude range shown in Figure 7).

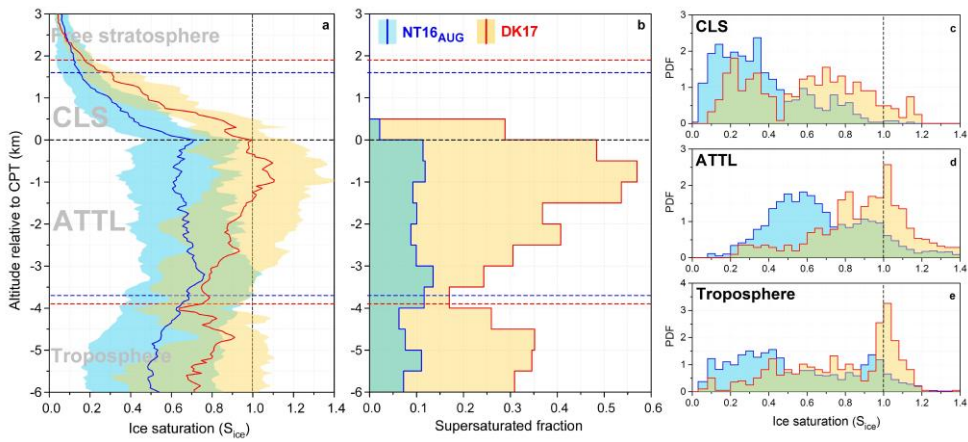


Figure 9. Panel a: mean profiles and standard deviation of ice saturation (S_{ice}) as a function of altitude relative to CPT, for NT16AUG (blue) and DK17 (red). Panel b: supersaturated fraction (i.e. fraction of measurements with $S_{ice} > 1$) as a function of altitude relative to CPT. Panels c, d, e: PDFs of ice saturation in the CLS, ATTL and Troposphere regions, respectively.

- Deleted: (
- Deleted:)
- Deleted: (
- Deleted:)
- Deleted: (
- Deleted:)
- Deleted: UT

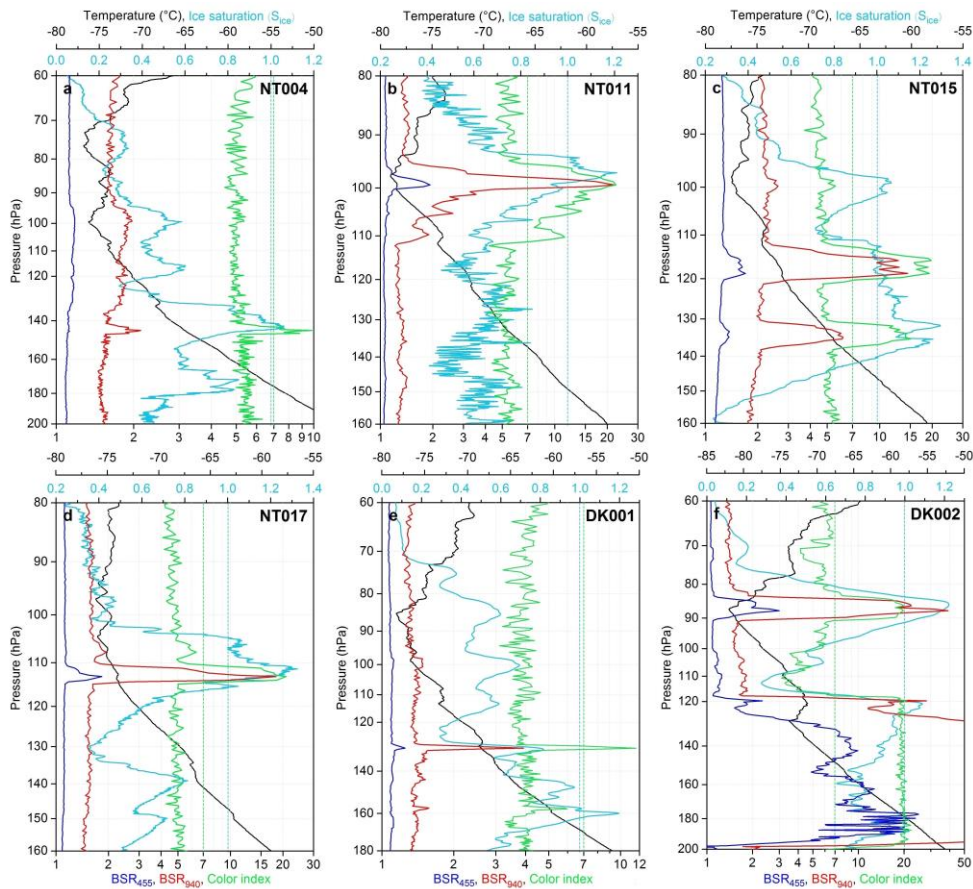


Figure 10. Examples of thin cirrus clouds measured during four individual soundings of the NT16_{AUG} campaign (panels a-d) and two soundings of the DK17 campaign (e, f). Solid lines show temperature (black), ice saturation (light blue), BSR at 455 nm (BSR_{455} , blue), BSR at 940 nm (BSR_{940} , red) and Color index (green). Vertical dashed lines mark the $S_{ice} = 1$ (light blue) and Color index = 7 (green) thresholds, used for cloud-filtering (see Section 6.1). Sounding identification numbers are noted in black on each panel (for date, time and payload of each sounding, see Table S1 in supplementary material).

Deleted: in the ATTL

Deleted: Panels

Moved down [8]: Sounding identification numbers are noted in black on each panel (for date, time and payload of each sounding, see Table S1 in supplementary material).

Moved (insertion) [8]

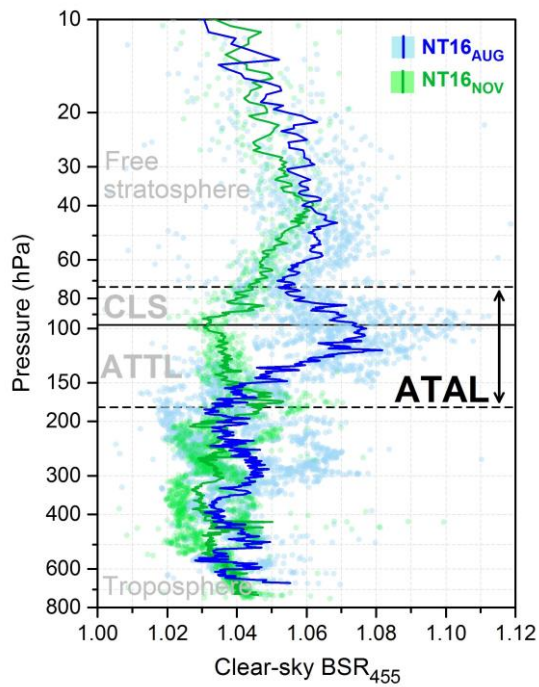


Figure 11. All clear-sky (i.e. aerosol-only) data points (dots) and mean profiles (solid lines) of BSR_{455} as a function of pressure, for $NT16_{AUG}$ (blue) and $NT16_{NOV}$ (green). Black dashed lines show the mean LRM (dashed), CPT (solid) and TOC (dashed) levels for $NT16_{AUG}$. The troposphere, ATTL, CLS and free stratosphere regions are identified by grey labels, and the ATAL region by a black arrow.

Deleted: , CPT and TOC levels for $NT16_{AUG}$. ¶

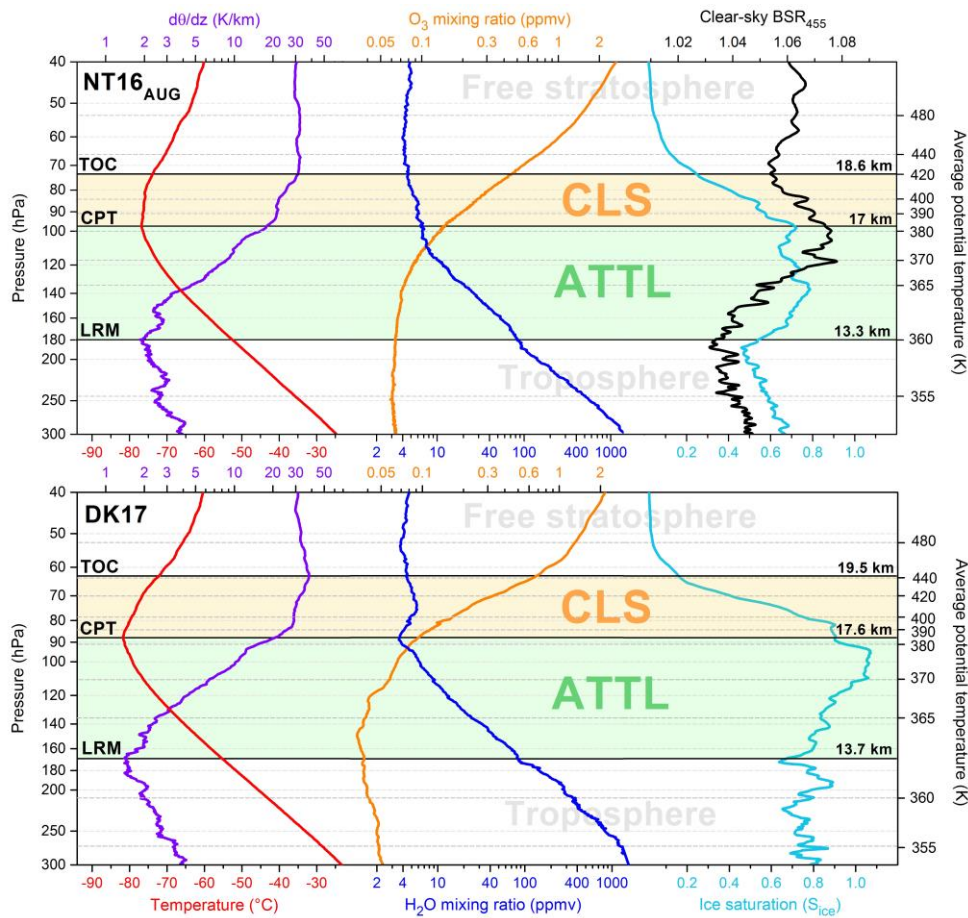


Figure 12. Mean profiles of temperature (red), $d\theta/dz$ (purple), H_2O mixing ratio (blue), O_3 mixing ratio (orange), ice saturation (light blue) and clear-sky aerosol BSR_{455} (black) as a function of pressure (left axis, light grey dashed lines) for NT16AUG (top panel) and DK17 (bottom panel). Average potential temperature levels are shown on the right axis and marked by dark grey dashed lines. Note that the pressure scale is the same for the two panels, and the potential temperature levels vary according to the measurements. The

Commented [BS9]: Former Figure 12 moved to Figure 6 and replaced with former Figure 13

Moved up [7]: Schematics of the vertical structure and main observed features of the UTLS above the southern slopes of the Himalayas. The Asian summer monsoon anticyclone (ASMA) consists of two layers, the Asian tropopause transition layer (ATTL) and the confined lower stratosphere (CLS). These layers are confined by three levels: the lapse rate minimum (LRM, green surface), the cold-point tropopause (CPT, red) and the top of confinement (TOC, blue).

Deleted: ¶
Figure 13.

Deleted: measured

Deleted: cyan

Deleted: green

average CPT, LRM and TOC levels are marked by black solid lines. The ~~A~~ TTL and ~~CLS~~ layers are highlighted by light green and orange shading, respectively. Note that mean profiles of $d\theta/dz$, ice saturation and clear-sky aerosol BSR_{455} are smoothed with a ± 5 hPa (about 250 m) moving average (same as in Figure ~~4~~).

Deleted: Asian

Deleted: (ATTL)

Deleted: Confined LS (

Deleted:)

Deleted: marked

Deleted: 6, Panel c